DEVELOPMENT OF ENDOSOME DISRUPTIVE PEPTIDE AND PEG CONJUGATE BASED DOXORUBICIN DELIVERY SYSTEM

A Thesis Submitted to
the Graduate School of Engineering and Sciences of
İzmir Institute of Technology
in Partial Fulfillments of the Requirements for the Degree of

MASTER OF SCIENCE

in Chemical Engineering

by
Selin ÖZKIYICI

July 2019
İZMİR

We approve the thesis of **Selin ÖZKIYICI**

Examining Committee Members:

Assist. Prof. Dr. Ayben TOP
Department of Chemical Engineering, İzmir Institute of Technology

Prof. Dr. Seher Fehime ÇAKICIOĞLU ÖZKAN
Department of Chemical Engineering, İzmir Institute of Technology

Assist. Prof. Dr. Çisem BULUT ALBAYRAK
Department of Food Engineering, Adnan Menderes University

19 July 2019

Assist. Prof. Dr. Ayben TOP
Supervisor, Department of Chemical Engineering,
İzmir Institute of Technology

Prof. Dr. Erol ŞEKER
Head of the Department of Chemical Engineering

Prof. Dr. Aysun SOFUOĞLU
Dean of the Graduate School of Engineering and Sciences

ACKNOWLEDGMENTS

Foremost, I would like to express my sincere gratitude to my advisor, Assist. Prof. Dr. Ayben TOP, for the continuous support during my M.Sc. study as well as for her motivation, enthusiasm, and immense knowledge. Her guidance helped me a lot throughout my research and writing of my thesis. I could not have imagined having a better advisor and mentor for my M.Sc. study.

I would also like to thank to my committee members, Prof. Dr. Seher Fehime ÇAKICIOĞLU ÖZKAN and Assist. Prof. Dr. Çisem BULUT ALBAYRAK for their valuable suggestions and recommendations.

Prof. Dr. Talat Yalçın are indebted for kindly performing MALDI-TOF mass spectroscopy experiments at Biological Mass Spectrometry and Proteomics Facility located at the Department of Chemistry. I really appreciate Dr. Hüseyin ÖZGENER for taking NMR data. I am grateful to Yekta GÜNAY and Filiz KURUCAOVALI for making dynamic light scattering experiments and HPLC analyses possible. I also appreciate Research Specialist Deniz ŞİMŞEK, Laboratory Technician Belgin TUNÇER KIRKAR, and Research Assistant Dildare BAŞALP from the Department of Chemical Engineering for their helps in characterization steps.

I am grateful to my lab mates Berk UYSAL, Damla YALÇIN, Emre DEĞİRMENCİ and Burcu SIRMA for their supports and contributions during my experiments.

I would also like to thank to TUBİTAK-Münir Birsel Foundation for the M.Sc. scholarship and İzmir Institute of Technology Scientific Research Projects Coordination Unit (BAP Project Number = 2017İYTE53) for the partial financial support of the project.

Finally, I want to thank to my family for giving me a chance to improve myself, and also for their unconditional love, endless courage and precious support.

ABSTRACT

DEVELOPMENT OF ENDOSOME DISRUPTIVE PEPTIDE AND PEG CONJUGATE BASED DOXORUBICIN DELIVERY SYSTEM

In this study, it was aimed to develop a drug carrier system including a TAT-derived cell penetrating peptide in order to provide fast transport of anticancer drugs from endosomal compartments to nucleus. The drug delivery system, denoted as mPEG-peptide-oxime-DOX, was based on polyethylene glycol, endosome disruptive peptide ($G_2RQR_3QR_3G_2S$), and doxorubicin (DOX) conjugate. Control drug delivery system, lack of the peptide (mPEG-oxime-DOX) was also synthesized to assess the effect of the peptide on the physiochemical and drug release properties of the drug carrier. As the first synthesis step, mPEG-OH was converted to mPEG-aldehyde form using DMSO-acetic anhydride oxidation reaction and aldehyde functionalization was determined by using FTIR and NMR spectroscopy. The peptide and mPEG-peptide were synthesized using solid phase synthesis protocol, and their purities were confirmed using HPLC and MALDI-TOF mass spectroscopy analyses. Prior to DOX conjugation, hydroxyl group of serine residue in the mPEG-peptide system was oxidized to aldehyde. The anticancer drug was attached to the carrier molecules via amine-aldehyde reaction forming an acid cleavable oxime bond. Drug release, size distribution, and stability of the PEG-peptide-oxime-DOX system were evaluated and compared with those results of the control drug delivery system. For mPEG-oxime-DOX, a pH programmed DOX release with the respective % DOX release values of ~68 % and ~28 % at pH 5.0 and pH 7.4 was observed. For mPEG-peptide-oxime-DOX, on the other hand, quite low DOX release (~10-15 %) was obtained for both pH values suggesting possible interaction between DOX and the peptide. Mean size value of the mPEG-oxime-DOX was measured as ~24 nm. However, mPEG-peptide-oxime-DOX, had quite lower hydrodynamic diameter values (~3nm and ~6 nm at pH 5.0 and pH 7.4, respectively) possibly due to repulsions between the arginines in the peptide domain. Observation of the morphology and evaluation of the cytotoxicity of these drug delivery systems are underway.

ÖZET

ENDOZOM PARÇALAYICI PEPTİD VE PEG KONJUGATI BAZLI DOKSORUBİSİN TAŞIYICI SİSTEMİ GELİŞTİRİLMESİ

Bu çalışmada, antikanser ilaçların endozomal bölmelerden çekirdeğe hızlı transferini sağlamak için TAT türevi bir hücre delici peptid içeren ilaç taşıyıcı sisteminin geliştirilmesi amaçlanmıştır. mPEG-peptid-oksim-DOX olarak adlandırılan ilaç taşıyıcı sistemi, polietilen glikol, endozom parçalayıcı peptid ($G_2RQR_3QR_3G_2S$) ve doksorubisin (DOX) konjugatı temellidir. Peptidin, ilaç taşıyıcının fizikokimyasal ve ilaç salım özelliklerine etkisini değerlendirmek için peptid içermeyen kontrol ilaç taşıyıcı sistemi de (mPEG-oksim-DOX) sentezlenmiştir. İlk sentez adımı olarak mPEG-OH, mPEG-aldehit formuna DMSO-asetik anhidrit oksidasyon reaksiyonu ile dönüştürülmüş ve aldehit işlevselleştirilmesi, FTIR ve NMR spektroskopisi kullanılarak belirlenmiştir. Peptid ve mPEG-peptid katı faz sentez protokolü ile sentezlenmiş ve HPLC ve MALDI-TOF kütle spektroskopi analizleri kullanılarak saflıkları teyit edilmiştir. DOX konjugasyonu öncesinde, mPEG-peptid sisteminde bulunan serin amino asitinin hidroksil grubu aldehite oksitlenmiştir. Antikanser ilaç, taşıyıcı moleküllere asit parçalanabilir oksim bağı ile bağlanmıştır. PEG-peptid-oksim-DOX sisteminin ilaç salımı, boyut dağılımı ve stabilitesi değerlendirilmiş ve kontrol sisteminin sonuçlarıyla karşılaştırılmıştır. mPEG-oksim-DOX için, pH 5.0 ve pH 7.4'te sırasıyla yaklaşık % 68 ve % 28 DOX salım değerleri ile pH programlı bir DOX salımı elde edilmiştir. Diğer taraftan, mPEG-peptid-oksim-DOX için her iki pH değerinde de oldukça düşük DOX salımı (yaklasık % 10-15) elde edilmiş ve DOX ile peptid arasındaki muhtemel etkileşimi sebebiyle olduğu düşünülmüştür. mPEG-oksim-DOX'un ortalama boyut değeri yaklaşık 24 nm olarak ölçülmüştür. Buna karşın, mPEG-peptid-oksim-DOX, muhtemelen peptid kısmındaki arjininler arasındaki itmeler nedeniyle, oldukça düşük hidrodinamik çap değerlerine (pH 5.0 ve pH 7.4 için sırasıyla yaklaşık 3 nm ve 6 nm) sahip olmuştur. Bu ilaç taşıyıcı sistemlerinin morfolojilerinin gözlenmesi ve sitotoksisitelerinin değerlendirmesine yönelik çalışmalar devam etmektedir.

TABLE OF CONTENTS

LIST OF FIGURES

LIST OF TABLES

NOMENCLATURE

FDA	US Food and Drug Administration
DOX	Doxorubicin
EPR	Enhanced Permeability and Retention
MDR	Multidrug Resistance
DDS	Drug Delivery System
MMPs	Metalloproteinases
PCI	Photochemical internalization
CPPs	Cell penetrating peptides
PTDs	Protein transduction domains
Arg	Arginine
Lys	Lysine
TAT	Trans activating transcriptional
TAX	Paclitaxel
NPs	Nanoparticles
MSNs	Mesoporous silica nanoparticles
SCL	Sulfatide-containing liposome
Cur	Curcumin
APEG	Allyl polyethylene glycol
mPEG	Methoxy polyethylene glycol
TPP	Triphenylphosphine
HA	Hyaluronic acid
LNPs	Lipid-nanoparticle assemblies
DMAB	Dimethyldidodecylammonium bromide
PLGA	Poly (lactic-co-glycolic acid)
CrO_3	Chromium oxide
PyBOP	Benzotriazol-1-yl-oxytripyrrolidinophosphonium hexafluorophosphate
DEE	Diethyl ether
DIEA	N,N-Diisopropylethylamine
DMSO	Dimethyl sulfoxide
DCM	Dichloromethane

TEA	Triethylamine
$CDCl_3$	Deuterated chloroform
TFA	Trifluoroacetic acid
mPEG-COH	Aldehyde Functionalized mPEG
SPPS	Solid phase peptide synthesis
Ser	Serine
FTIR	Fourier Transform Infrared Spectroscopy
KBr	Potassium bromide
NMR	Nuclear Magnetic Resonance
HPLC	High Performance Liquid Chromatography

CHAPTER 1

INTRODUCTION

In this chapter, properties of cancer cells and conventional cancer treatment methods were explained. Characteristics of ideal drug delivery systems were described by taking account into enhanced permeation and retention (EPR) and multidrug resistance (MDR) effects. Additionally, endosomal escape mechanism was illustrated and exploitation of cell penetrating peptides (CPP) in the transportation of cargoes was discussed. Finally, the drug delivery system containing an endosome disruptive TAT-derivative peptide developed in this study was introduced, and contents of the chapters of this thesis were presented.

1.1. Cancer and Cancer Cells

Cancer is a series of molecular events, which occur by uncontrolled growth and spreading of abnormal cells in the body. Human bodies produce more than hundred millions of cells. DNA of these cells includes different types of genes that give information to the cells about how to behave. Many of the normal cells have ability to create new cells by dividing. When genes of some cells change, these cells start to grow and divide continuously bypassing the normal cell cycle, and hence, become cancer cells (Treatments & Side Effects, 2014). Figure 1.1 shows the difference between the division mechanism of the normal and cancer cells. While the normal cells reproduce themselves only when and where needed and stick together in the right place in the body, cancer cells have no programmed death ability resulted in the accumulation of the abnormal cells forming tumor tissues. Additionally, cancer cells can also spread to the other parts of the body travelling through the blood or lymph systems.

The exact mechanism of formation and spreading of cancer is still not well understood but external factors, such as chemicals, radiation and infection, and internal

factors including inherited metabolism mutations, hormones and immune conditions are likely to initiate and boost carcinogenesis (Feng & Chien, 2003).

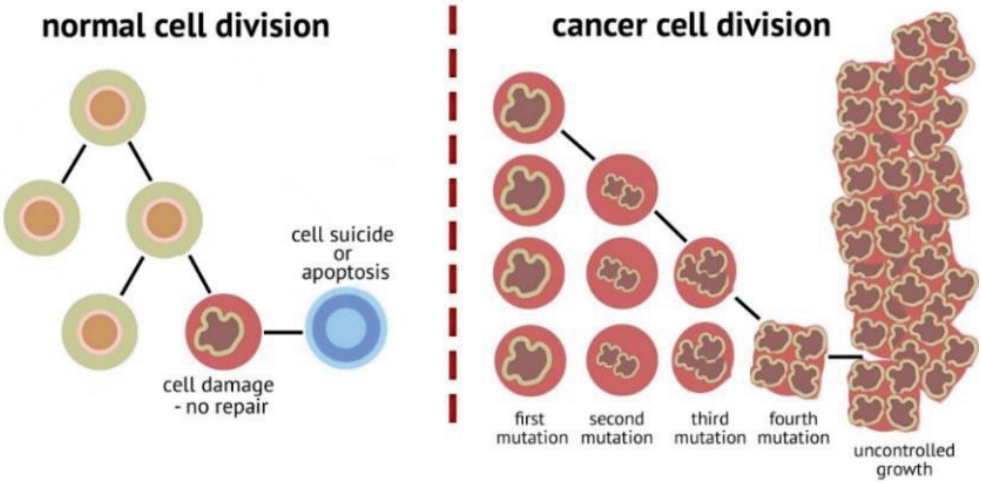

Figure 1.1. Normal cell and cancer cell division behavior

1.2. Conventional Cancer Treatment Methods

Cancer treatment methods are selected according to the type, location and stage of cancer with a purpose of curing and controlling the disease or mitigating its symptoms. The most common conventional treatment methods are surgery, radiation therapy and chemotherapy. Surgery and radiotherapy are recommended methods to destroy solid tumors but they fail to control metastatic cancer types. Chemotherapy, on the other hand, is the destruction of cancer cell by using drugs which are often toxic or life-threatening and it is the most common method to cope with metastasis. The chemotherapeutic drugs can be administered by orally or mostly intravenously. The efficiency of this treatment depends on the activity, dosage and form of the drug used and patient condition. Especially, it is crucial to apply necessary dosage of the drug and once accumulated in the tumor cells, the drug should stay there for a certain time period to exhibit its activity (Treatments & Side Effects, 2014).

The idea behind the use of toxic drugs is to damage the cancer cell so that they cannot spread but these toxic drugs used can kill some healthy cells in the body, as well. Additionally, most drugs are hydrophobic i.e. they are not soluble in water but non-

aqueous solvents used to disperse the drugs may also be cytotoxic. Other common side effects of chemotherapy are myelosuppression, nerve damage, diarrhea, mouth sores, organ dysfunction, alopecia, nausea and decrease in the number of blood cells (Feng & Chien, 2003; Kalyane et al., 2019).

Over 100 anticancer drugs have been approved by the US Food and Drug Administration, (FDA) such as bleomycin, daunomycin, docetaxel, doxorubicin, idarubicin, mitomycin (Carvalho et al., 2009; Feng & Chien, 2003). The most popular chemotherapeutic drug family is anthracyclines and commonly used type of drug is doxorubicin (DOX), with a chemical structure given in Figure 1.2. The mechanism of anticancer activity of DOX is quite complex and has not been completely understood. However, it is clear that this type of cancer drugs intercalates into DNA by inhibiting the activity of topoisomerases (primarily topoisomerase I and II), which unwind DNA during replication process. The dose of DOX should be carefully controlled because of the unwanted effects of this toxic chemotherapeutic drug in different organs as it does not show specific activity solely in tumor cells but it can affect proliferation of the healthy cells in the body as well. The main side effect of DOX is its well-known cardiotoxicity, which can be resulted in acute or chronic effects. Although cardiotoxic effect of DOX is the driving force for improving design strategies, its toxicity to other organs such as brain, liver and kidney is the other important problem. (Tacar et al., 2013). In order to reduce its associated side effects and to improve therapeutic activity of DOX, nanosized drug carrier systems have been developed to direct the drug specifically to the tumor site by exploiting enhanced permeability and retention (EPR) effect.

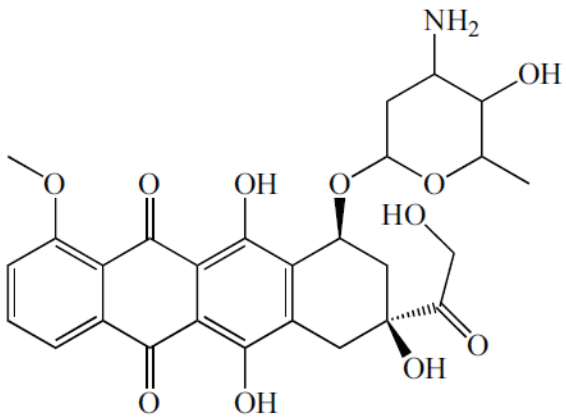

Figure 1.2. Chemical structure of doxorubicin

(Source: Carvalho et al., 2009; Kobayashi et al., 2013)

1.3. Ideal Drug Delivery Systems

Anomalous growth of tumor cells triggers overexpression of proangiogenic factors due to the increased requirement of nutrients and oxygen. As a result, new tumor vasculature system emerges with a number of defects such as irregular and leaky blood vessels, blind ends, disorganized endothelial cells and lack of basement membrane or the smooth-muscle layer (Kobayashi et al., 2013). The differences in the structure of the vasculature of normal and cancer cells are given in Figure 1.3 (Brown & Glaccia, 1998). Leakiness in the tumor blood vessels allows blood plasma components, especially, macromolecules to reach tumor site more selectively. Additionally, lymphatic drainage system does not function properly in tumor tissues, which ensures macromolecules to retain in the tumor site. (Iyer et al., 2006).

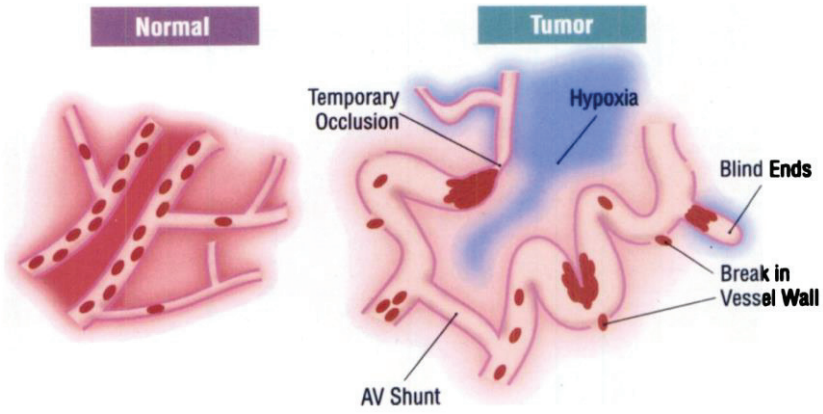

Figure 1.3. Structure of vasculature system of normal and cancer cells

(Source: Brown & Glaccia, 1998)

Hence, it is so called 'enhanced permeability and retention (EPR) effect' that facilitates macromolecule accumulation in tumors because of the anatomical defectiveness of tumor tissues. It was reported that exploitation of EPR effect as a passive tumor targeting strategy was mainly dictated by the molecular weight of the carrier macromolecules or size of nanoparticle vehicles. As it can be seen from Figure 1.4, the carrier systems having sizes between 10 and 200 nm (or macromolecules with molecular weights between 40 and 800 kDa), are more likely to accumulate in tumor tissues due to lack of lymphatic clearance and smooth layer in tumor tissues, and more porous blood vessels (Greish, 2010; Kalyane et al., 2019; Nakamura et al., 2016). Small molecules such

as low molecular weight drugs, on the other hand, diffuse easily in and out of both normal and tumor blood vessels so cannot be selectively retained in tumor site. The EPR effect was first described in 1986 by extravasation of Evans blue complex with albumin into solid tumor tissues in mouse. It was also observed for a variety of molecules including highly biocompatible plasma proteins, synthetic biocompatible polymers of HPMA and lipid particles (Maeda et al., 2016).

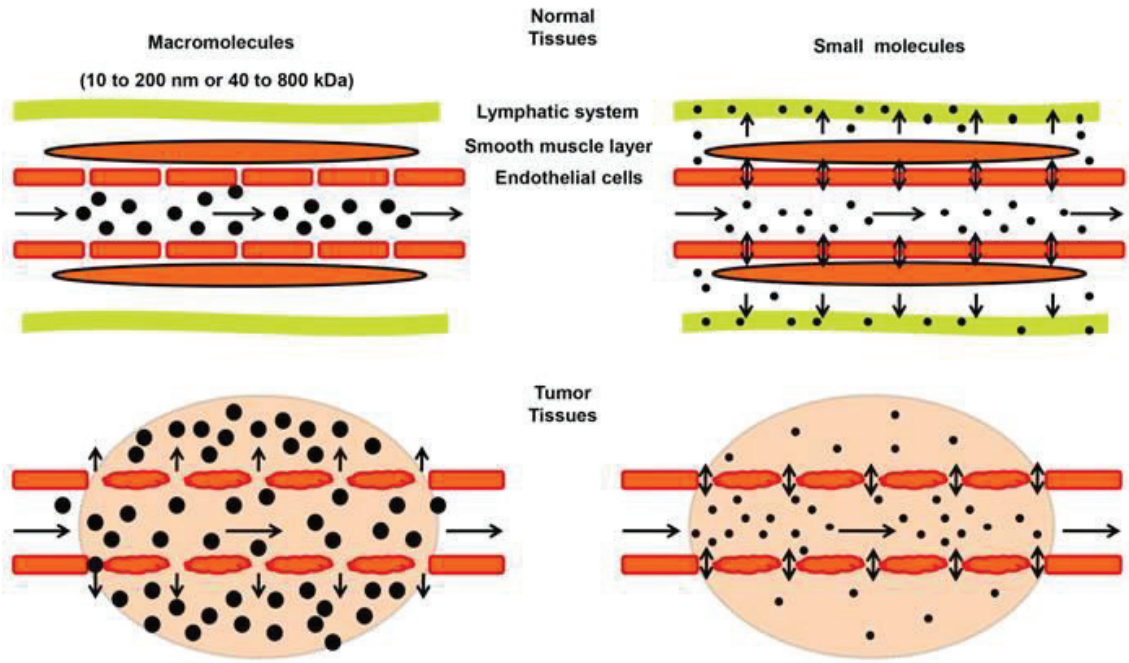

Figure 1.4. Schematic representation of EPR effect

(Source: Greish, 2010)

Decreased drug uptake, increased drug efflux, activation of detoxifying systems, superior DNA repair mechanisms and defective apoptosis pathways can cause cancer cell to be resistant to anticancer drugs, which is known as multidrug resistance (MDR) (Daglioglu, 2017; Mihanfar et al., 2019; Sun et al., 2014; Yin et al., 2013). The MDR in cancer cells was reported to be related to the overexpression of P-glycoprotein (Brigger et al., 2002). These efflux transporters pump chemotherapy drugs out of the cell so that intracellular concentration of drugs in cancer cells gets lower. The schematic representation of P-glycoprotein transporter is given in Figure 1.5 (Sun et al., 2014). Increasing the serum dosage of the drug can be one solution of the MDR but this method can also be resulted in inevitable toxic effects of the drug on normal tissues, as well. For this reason, designing new drug delivery systems that ensure fast release of drug has been taken account into consideration to cope with MDR (Daglioglu, 2017).

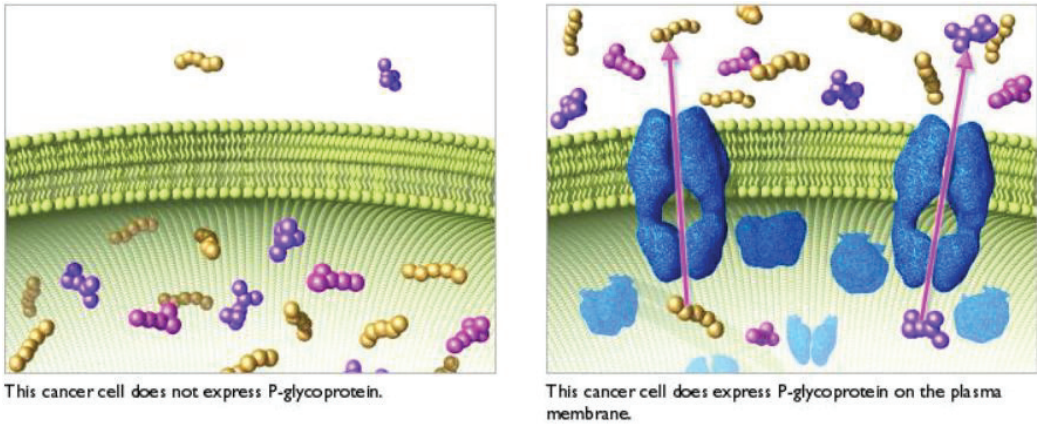

Figure 1.5. The schematic representation of P-glycoprotein transporter

Unconjugated or uncoated (bare) drugs can be absorbed, disturbed or excreted after the administration process so that the fate of the drug becomes difficult to control and most of the time, its therapeutic dose cannot be reached at the desired tissue. It was well documented that application of the drug at optimal dose and at the right site of the body was of paramount importance to achieve a therapeutic dose and to avoid side effects of the drug. Thus, drug delivery systems (DDSs) with the following characteristics designed should not only provide programmed release but also ensure transportation of the drugs into the target site (Drug Delivery Systems,2014):

- Increase drug bioavailability
- Provide controlled drug delivery
- Transport the drug intact to action site while avoiding non-diseased host tissues
- Provide high degree drug dispersion
- Provide minimal drug leakage during the transit

A number of drug delivery systems have been proposed such as drug conjugates, liposomes, nanoparticles, and micellar aggregates, which are mostly based on self-assembled amphiphilic block copolymers to host chemotherapeutic drugs (Torchilin, 2007; Yin et al., 2013). In order to exploit the EPR effect and, hence, to provide passive targeting, nanoparticles including liposomes, micelles (10-100 nm), nanospheres (100-200 nm), and nanocapsules (100-300 nm) have been used to encapsulate, adsorb or disperse the drugs as the uptake mechanism of these carriers is directly related to size of particles (Letchford & Burt, 2007).

One of the commonly explored group of DDSs is pH responsive systems which exploit the pH gradient in the tumor cells. The pH values in solid tumors were reported as 6.8-7.2, 5-6 and 4.5-5.5, for the cytoplasm, endosomes and lysosomes, respectively (Kanamala et al., 2016; Mura et al., 2013; Pecot et al., 2011; Schmaljohann, 2006; Yin et al., 2013). These DDSs stabilize the drug at physiological pH but are designed to release it in the acidic intracellular compartments. pH responsiveness can be imparted either by the incorporation of ionizable functional groups such as amine or carboxylic acid groups into the carrier system or by the introduction of acid cleavable linkage between the drug and the carrier system. (J. Liu et al., 2014; Yin et al., 2013). For example, carboxylic groups in the carrier molecules can act as binding sites for cationic drugs. These drugs can be loaded to the DDS by electrostatic interactions forming ion-pair complexes, and release of the drugs occurs at acidic pH, as a result of the rupture or weakening of the drug-carboxylic group interactions (Yin et al., 2013). The acid sensitive bonds such as hydrazone and oxime bond can also provide effective release of the drugs in the acidic environments of endosomes and lysosomes (Kaneo et al., 2013).

Enzyme responsive DDSs are another family DDSs, which exploit overexpression of certain enzymes in tumor cells. Expression levels of some of the enzyme hydrolases such as proteases, esterases and glucosidases in tumor cells are much higher than those of normal cells so that these enzyme concentration differences can be used to promote the release of the drug (Shah et al., 2018). Several enzymes such as matrix metalloproteinases (MMPs), cathepsin B, hyaluronidase, and azoreductase serve as triggers in the enzyme responsive DDSs (Kuang et al., 2015). Polymeric materials, phospholipids and inorganic materials have been reported to be modified with substrates of these enzymes to be used as enzyme sensitive drug delivery systems (Q. Hu et al., 2014).

1.4. Endosomal Escape Mechanism

Attainment of therapeutic activity of drugs depends on efficient delivery of these agents to the target cells. However, macromolecular delivery systems having sizes greater than 1,000 Da with no bioavailability can hardly cross the cell membrane and enter the cells, which causes retardation of the delivery of therapeutics into cells. These macromolecular systems are usually taken up by the cells via endocytosis. The critical

step of endocytosis, which dictates the ultimate therapeutic effect is translocation of the drugs from endosomes to cytosol. For this reason, the development of technologies to accelerate the transportation of therapeutic molecules especially to cytosol and nucleus, is required.

Endocytosis is uptake mechanism of cells which starts with entrapment of the foreign molecules by endosomes and end up with their digestion in lysosomes as shown in Figure 1.6. (Varkouhi et al., 2011; Yin et al., 2013). In the first stage, a macromolecule is surrounded by plasma membrane of the cell forming a vesicle called early endosome. Then, these internalized macromolecules are received by late endosome in order to mediate the order of events. In the last stage of the endocytosis, macromolecules transferred from the late endosome are digested by hydrolytic enzymes in lysosomes thereby hindering the activity of the macromolecules or the therapeutic agents associated with the macromolecules. Therefore, endosomal release of macromolecules is necessary before lysosomal digestion. (Varkouhi et al., 2011).

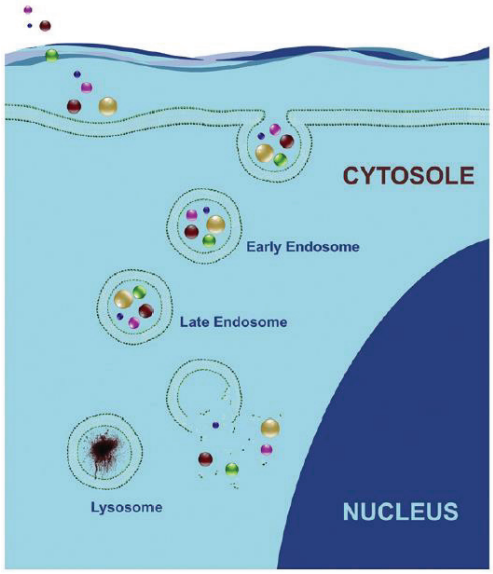

Figure 1.6. A representation of endocytosis

(Source: Varkouhi et al., 2011)

Endosomal escape mechanisms occur in a number of ways such as pore formation in endosomal membrane, pH-buffering effect (proton sponge effect), fusion in the endosomal membrane, and photochemical disruption of the endosomal membrane. Pore formation in the lipid membrane is usually observed as a result of internal stress or

internal membrane tension induced by binding of agents such as cationic amphiphilic peptides (AMPs) to the lipid bilayer. The agents, which have high buffering capacity and ability to swell in protonated form, on the other hand, cause proton sponge effect. Protonation of these agents occurs in the low pH environment in endosomes. Then, ions (Cl^- and H^+) and water start to flow into the endosomal environment extensively triggering the osmotic swelling and rupture of the endosomal membrane and, hence, release of the entrapped components, as given in Figure 1.7 (Varkouhi et al., 2011). Endosomal escape by fusion is the destabilization of endosomal membrane by the action of fusogenic peptides which are typically 20-30 amino acids long and hydrophobic (V. Munsell et al., 2016). Another endosomal escape mechanism, the photochemical disruption or photochemical internalization (PCI) is mediated by a photosensitizing compound which localizes in endocytic vesicle and causes photochemical damage in the membrane and, hence, release of macromolecules into cytosol upon exposure to light (Prasmickaite et al., 2002).

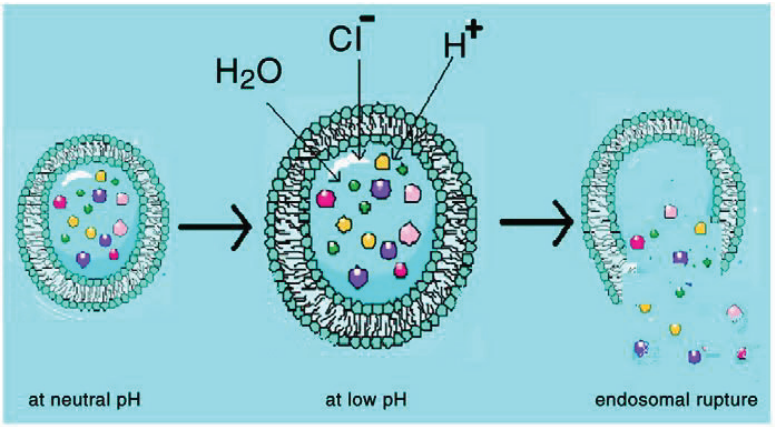

Figure 1.7. The schematic representation of proton sponge effect

(Source: Varkouhi et al., 2011)

A number of proteins, peptides and chemical agents have been purified or synthesized as endosomal escape agents to provide endosomal escape of macromolecules effectively. Protein and peptide based endosomal escape agents are usually derived from several viruses and bacteria proteins (Varkouhi et al., 2011). Of these agents, cell penetrating peptides (CPPs) also known as protein transduction domains (PTDs), are short peptide sequences with rapidly internalized positive charge enabling the transport of cargoes. The cargo consists of either a low molecular weight drug or a macromolecule

which does not easily cross to cell membrane by itself. Thus, the main function of CPPs is to enhance the cellular uptake of these macromolecules. The major drawbacks of these peptides are the lack of cell type selectivity and low plasma half-life due to the enzymatic degradation (Böhmova et al., 2018).

CPPs can be classified according to chemical structure, nature of the parent protein and mechanism of cell entry. Cationic, amphipathic or hydrophobic peptides have the ability to penetrate through the cell membrane. The cationic groups of CPPs are positively charged at physiological pH and these peptides rich in arginine (Arg) and lysine (Lys). Perhaps, oligo-arginines are the mostly studied group of peptides. It was reported that minimum eight arginine was required to provide cell membrane penetration. (Böhmova et al., 2018; Guidotti et al., 2017). Another class of CPPs is TAT-derived peptides containing multiple Arg and Lys residues, which act as a nuclear localization sequences (NLSs). This NLSs can deliver various cargoes into cell nucleus. TAT peptide is the first and best characterized CPPs peptide that comes from HIV-1 trans activating transcriptional (TAT) protein (V. Munsell et al., 2016). It is a highly cationic type of CPP because of 6 Arg and 2 Lys in the sequence (Schmidt et al., 2010).

Cargoes can be in the forms of covalently or non-covalently attached to CPPs during their transportation. Both systems have advantages or disadvantages so the choice of type of the attachment is dependent on particular structures of CPPs and cargo. Covalent attachment is the most commonly used method, in which cargoes are conjugated to CPPs via chemical linkage mainly amide, disulfide or thioester bonds. Spacers can also be attached to side chain of the functional groups of CPPs, such as lysine amino group or carboxylic acid or amino group at the respective C or N terminus of peptide to optimize the distance between CPPs and cargo (Böhmova et al., 2018). In the covalent attachment, on the other hand, possibility of the change in the biological activity of conjugated molecules should be considered (Guidotti et al., 2017). Hydrophobic or electrostatic interactions between positively charged CPPs and negatively charged cargoes form non-covalent bonding. Although non-covalent bonding can provide a protection of bioactive peptides from enzymatic degradation, stability of the complex may become lower in vivo. (Böhmova et al., 2018; Guidotti et al., 2017).

In this study, it was aimed to incorporate TAT-derived cell penetrating peptide into a drug carrier system to ensure fast transport of the anticancer drug to the cytoplasm, and finally, to the nucleus. The DDS was based on the of PEG-peptide conjugate and the model drug, doxorubicin was attached to the system via acid cleavable oxime bond. Drug

release, size, and stability properties of the PEG-peptide-oxime-DOX system were evaluated and compared with those of the control DDS lack of peptide sequence, mPEG-oxime-DOX.

In the following literature review chapter (Chapter 2), examples of responsive DDSs proposed for cancer therapy along with the ones containing endosome disruptive properties were provided.

In Chapter 3, materials and synthesis procedures used to prepare the DDSs developed in this study (mPEG-peptide-oxime-DOX and mPEG-oxime-DOX) were given. Methods applied to characterize the carrier molecules and DOX-conjugated DDSs were described.

In Chapter 4, FTIR and NMR characterization results of the functional mPEGs synthesized in this study were presented. Purities of the TAT-derived peptide and the mPEG-peptide conjugate were assessed. Size, stability, and DOX release results of the prepared DDSs were provided.

Chapter 5 concludes this thesis with the most striking results of this study. Additionally, future experimental plans were outlined.

CHAPTER 2

LITERATURE REVIEW

In this chapter, examples of drug delivery systems developed for cancer therapy including responsive DDSs and endosome disruptive sequence containing DDSs were presented. Recent studies about PEG-peptide containing DDSs synthesized by our research group were summarized.

2.1. Nanoparticulate Drug Delivery Systems

A variety of nanoparticulate systems including micelles, liposomes, and nanospheres have been designed as drug delivery systems for the protection and transportation of toxic drugs thereby increasing the blood circulation time of the drugs as well as providing passive targeting to cancer cells. Although polymeric drug delivery systems dominated in this area, in recent years, inorganic nanoparticles coated with small molecules or polymers have also been developed.

One of the examples of polymeric nanoparticulate DDSs is mPEG-PLGA copolymer micellar system developed for the co-delivery of doxorubicin (DOX) and paclitaxel (TAX). mPEG-PLGA nanoparticles (NPs), NPs-DOX, NPs-TAX and NPs-DOX-TAX were prepared by double emulsion method and emulsion/evaporation methods. Mean particle sizes of mPEG-PLGA-NPs, NPs-DOX and NPs-DOX-TAX were obtained as 22.83 ± 10.72 nm, 229.67 ± 13.27 nm, 243.63 ± 12.36 nm, respectively. TEM image of NPs-DOX-TAX given in Figure 2.1 indicated core-shell structure of the nanoparticles. In vitro release profiles of the drugs obtained at different pH values (4.4 and 7.4) showed that almost all of DOX and half of TAX released from the micelle within 50 h independent of pH (Figure 2.1). Both drugs were taken up effectively by the cells and suppressed the tumor cells growth more efficiently than the single drug at the same concentration. These results suggested that mPEG-PLGA nanoparticle systems could

provide co-delivery of different anticancer drugs with improved therapeutic potential. (Wang et al., 2011).

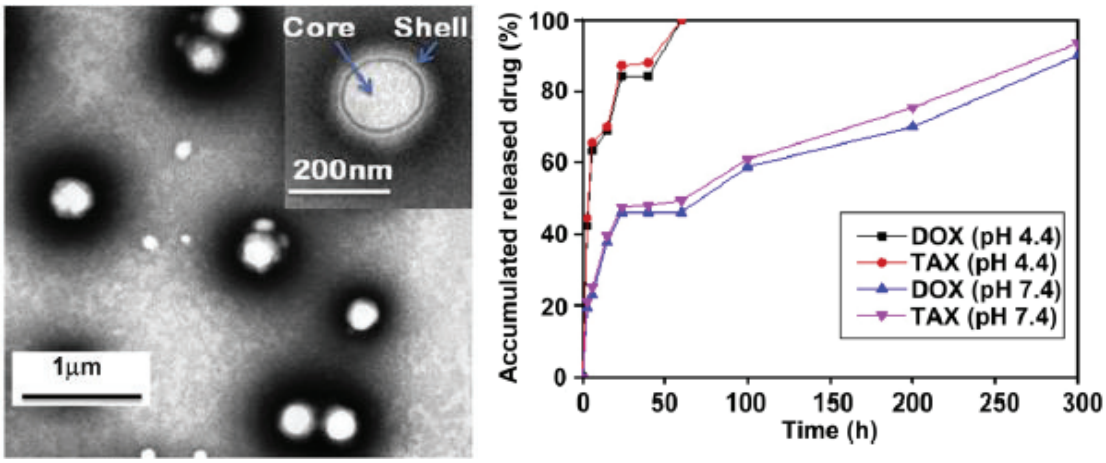

Figure 2.1. a) TEM image and b) drug release profiles of DOX-TAX loaded nanoparticles developed by Wang et al. (2011)

In the study of Hu et al. (2014), chitosan conjugated MCM-41-type mesoporous silica nanoparticles (CS-MSNs) with high loading capacity were prepared to encapsulate doxorubicin. In order to impart pH responsiveness to the silica nanoparticles and to prevent their aggregation in aqueous solutions, chitosan was conjugated to silica surface, which was modified with an amine-reactive linker molecule, 3-glycidyloxypro-pyl) trimethoxysilane. In the TEM image, highly ordered hexagonal arrays of MSNs with an average diameter of particles around 120 nm (15% polydispersity) were observed as given in (Figure 2.2). DOX release profiles of CS-MSNs were determined at different pH values. It was obtained that decreasing of media pH provided higher level of DOX release from nanoparticles due to the protonation of the amine groups of the chitosan. Maximum cumulative release of DOX was obtained as 75.4 % at pH 4.0. In vitro cytotoxicity of the nanoparticles was investigated by using MCF-7 breast cancer cells. CS-MSNs showed no cytotoxicity but DOX loaded CS-MSNs exhibited an increasing cytotoxicity effect over time causing approximately 50% cell death ratio at the end of 48 h. According to these results, DOX loaded CS-MSNs were proposed as smart nanoparticles for cancer treatment due to their pH-responsiveness. However, cytotoxicity tests have not been performed for free doxorubicin. Due to the lack of the positive control experiments, it is not possible to comment of the effectiveness of the cytotoxic activity of the CS-MSN based drug delivery systems (X. Hu et al., 2014).

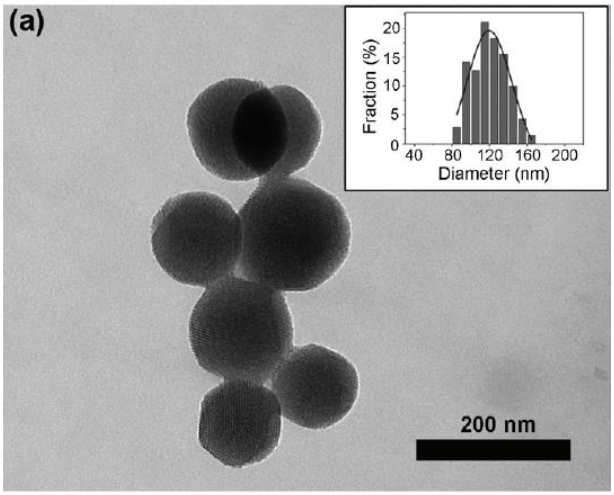

Figure 2.2. TEM image of MSNs developed by Hu et al. (2014)

In another study related to inorganic nanoparticles, oxidized mesoporous carbon nanospheres with high drug loading capacity were PEGylated (oMCN-PEG). First, MCNs were synthesized by using phenolic resol and pluronic F127 and oxidized to form oMCNs by hydrogen peroxide treatment. DOX was loaded into the pores of oMCNs, and then, the nanoparticles were coated with DSPE-mPEG 2000 to make them hydrophilic. The morphology of the nanoparticles was monitored by using high resolution TEM and TEM image is given in Figure 2.3. Spherical morphology, uniform diameter (about 90 nm) and well-defined mesoporous structure (about 3 nm mesoporous size) were obtained for MCNs. Similarly, a spherical morphology and monodispersed (95 nm) size distribution were observed for oMCNs. PEG-coating of oMCNs, appeared as ~5 nm thick shell layer. Additionally, pore volume and pore size values were obtained as 0.55 cm^3/g, 0.63 cm^3/g and 3.1 nm, 3.9 nm for MCNs, and oMCNs, respectively. Due to their higher pore volume and wider pores, oMCNs exhibited slightly higher drug loading capacity (about 38%) than MCNs (about 30%). Drug release profiles of DOX loaded oMCNs-PEG indicated that 8.7% and 42% of DOX were released at pH 7.4 and pH 5.5, respectively. At high DOX concentration (4 μg/mL), cytotoxicity of DOX loaded oMCN-PEG was found to be similar to that of free DOX. These results showed effective uptake of drug by the tumor cells (Wang et al., 2016).

Modified liposomal nanocarrier systems with programmed release ability have also been developed. In one of such studies, DOX was encapsulated in tumor microenvironment targeting sulfatide-containing liposomes (SCL), and therapeutic

activity of the SCL systems was evaluated in vitro and in vivo using BALB/c nude mice HT-29 tumor xenograft model. In vitro cell cytotoxicity of DOX, SCL and SCL-DOX

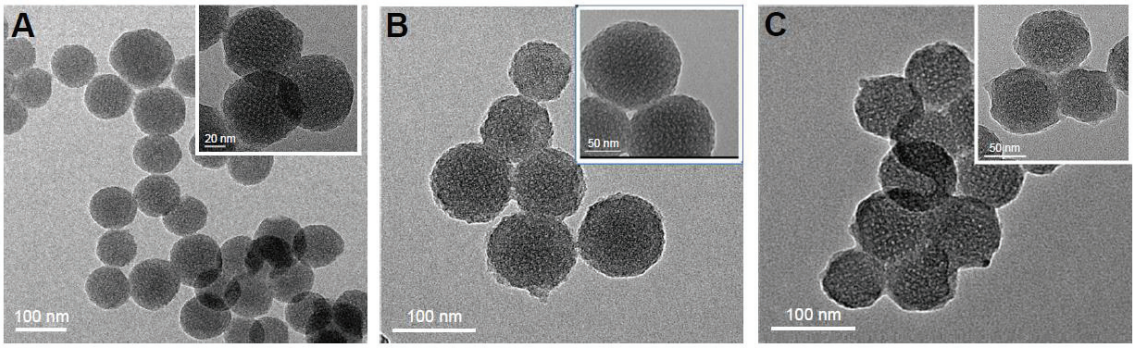

Figure 2.3. TEM images of MCNs, oMCNs and oMCNs-PEG developed by Wang et al. (2016)

was determined against HT-29 cells for 48 h. Dox-free SCL did not show any cytotoxic effect on the cells. Free DOX (IC50 value = 1.74 ± 0.10 μg/mL) had more toxicity than SCL-DOX (IC50 value = 2.77 ± 0.06 μg/mL). DOX-loaded SCL was injected to tumor-bearing mice and tumor volumes were determined as given in Figure 2.4. Final tumor volume values were obtained as 586.52 ± 29.63mm^3 and 809.13±43.75mm^3 for SCL-DOX and free DOX, respectively. The difference in tumor growth was attributed to enhanced permeability and retention effect exploited by the nanosized SCL carrier system. As a result, this study demonstrated that SCL-DOX showed enhanced toxicity profile for treatment of cancer (J. Lin et al., 2012).

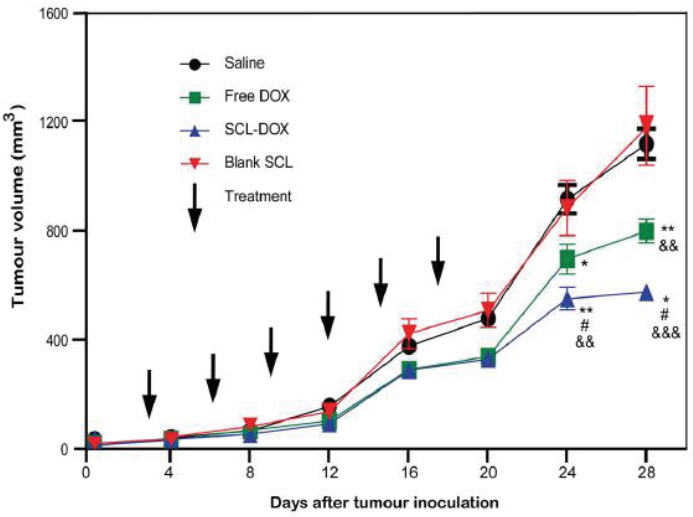

Figure 2.4. Tumor volume profiles of free DOX, blank liposomes (SCL) and DOX-loaded liposomes (SCL-DOX) developed by Lin et al. (2012)

2.2. pH Responsive Drug Delivery Systems

pH responsive DDSs can be obtained either by the introduction of acid cleavable bonds or incorporating pH responsive functional groups to the carrier molecules. The most popular acid cleavable bonds were reported as hydrazone and oxime bonds. Ionizable functional groups such as imidazole, amine and carboxylic acids, on the other hand, can also impart pH responsiveness to the DDSs without any chemical linkage between the drug and the carrier system. Both polymeric and inorganic nanoparticles based pH programmed systems have been developed.

As an example of polymeric pH responsive systems with acid cleavable bonds, Zhang et al (2016), proposed mPEG prodrug nanoparticles for co-delivery of DOX and curcumin (Cur). In this system, DOX was conjugated to mPEG via oxime bond that formed between aldehyde group of mPEG and amine group of DOX and Cur was loaded to the nanoparticles of mPEG-DOX conjugate. DOX and Cur release profiles of nanoparticles (PEG-DOX-Cur) in PBS including Tween 80 at different pH values are given in Figure 2.5. At pH 5.0 and at the end of 24 h, % release values of DOX and Cur were obtained as approximately 70% and 80%, respectively. At pH 7.4, on the other hand, less than 15% DOX and Cur release was observed clearly indicating pH responsiveness of the system. In vitro cytotoxicity of the conjugates was investigated using HEPG2 and HELA cancer cells. It was shown that at high concentrations of anticancer drugs, PEG-

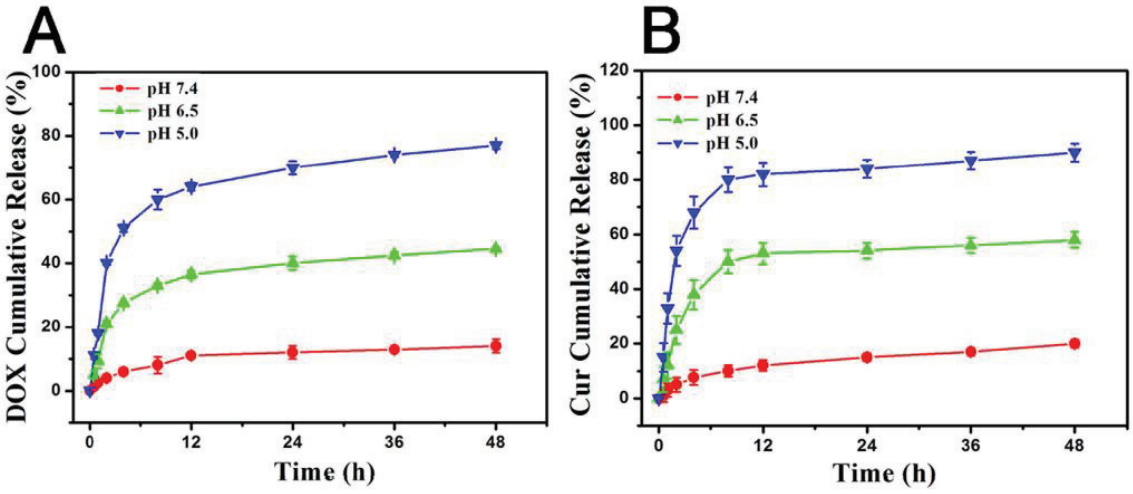

Figure 2.5. pH programmed a) DOX, and b) curcumin release profiles of mPEG-prodrug nanoparticles developed by Zhang et al. (2016)

DOX-Cur nanoparticles exhibited higher cytotoxic activity than free DOX, free Cur, free DOX/Cur and mPEG-DOX. (Zhang et al., 2016).

It is also possible to prepare dual responsive systems. For instance, Sang et al (2019) prepared pH and thermo-responsive polymeric micelles based on copolymers poly (N-isopropylacryamide-co-allyl poly (ethylene glycol)]-b-poly (γ-benzyl L-glutamate) (PNIPAM-co-APEG)-b-PBLG). Thermo-responsiveness was imparted by poly (N-isopropyl acrylamide) (PNIPAM) block and doxorubicin was covalently conjugated to the carrier copolymer via pH responsive hydrazone linkage. Drug release properties of the DDS were investigated by changing pH of the buffer solutions and the resultant profiles are shown in Figure 2.6. At the end of 72 h, % drug release values were obtained as 14% to 62% for the pH values of 7.4 to 4.0, respectively. Cytotoxicity evaluation of polymeric micelles, DOX-conjugated micelles and free DOX was performed by using HELA cells. DOX-free micelles did not show any cytotoxic effect. Although IC50 value of free DOX is lower than DOX-conjugated DDS, at high equivalent drug concentrations, the differences in the cytotoxic activity of free DOX and the DDS decreased. In conclusion, these thermo/pH dual-responsive polymeric micelles were proposed as promising drug delivery systems for cancer therapy. (Sang et al., 2019).

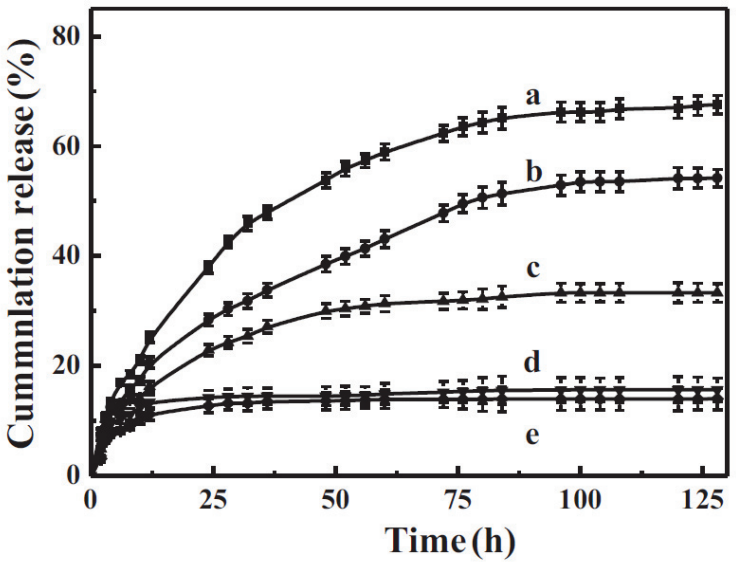

Figure 2.6. DOX release profiles of the dual-responsive polymeric micelles developed by Sang et al. (2019) at a) pH = 4.0, b) pH = 5.0, c) pH = 6.0, d) pH = 7.0, e) pH = 7.4

In another study, pH responsive drug delivery systems were obtained by grafting poly (L-histidine) to amine functionalized mesoporous silica nanoparticles (MSN-NH_2)

via surface-initiated ring opening polymerization. In this system, histidines with ionizable groups were used to control drug release. Two different pH responsive nanoparticles were synthesized by using 0.8 g and 1 g of Trt-His-NCA per 100 mg of MSN-NH_2 in polymerization reactions, denoted as MSN-PHis-1 and MSN-Phis-2, respectively. DOX was loaded to the nanoparticles by pH dependent procedure; first by mixing DOX and nanoparticles at pH 3 and then by increasing pH to 8. DOX release from the nanoparticles was investigated at physiological (7.4), mildly acidic (6.5) and acidic (5.0) pH values. The results of the drug release experiments are given in Figure 2.7. For MSN-NH_2, maximum release was obtained as 21% after 72 h incubation period at pH 5.0. At physiological pH, % drug release values were obtained as 23.1% and 10.7% at the end of 72 h for MSN-Phis-1 and MSN-Phis-2, respectively. At pH 5.0, on the other hand, respective % release values of MSN-Phis-1 and MSN-Phis-2 were obtained as 46.5% and 49.5% confirming pH responsive property of polyhistidines (Bilalis et al., 2016).

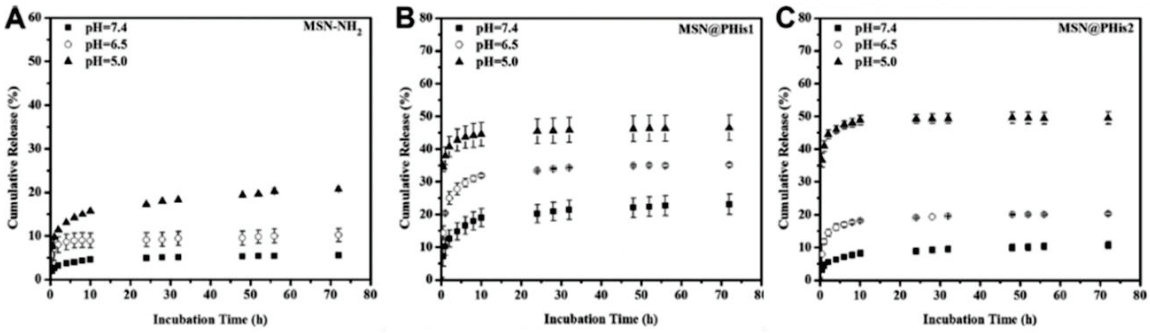

Figure 2.7. DOX release profiles of a) MSN-NH_2, b) MSN-PHis-1 and c) MSN-PHis-2 systems developed by Bilalis et al. (2016) at physiological (7.4), mild acidic (6.5) and acidic (5.0) pH environment

2.3. Enzyme Responsive Drug Delivery Systems

Enzyme responsive drug delivery systems can be obtained by incorporating substrate sequences of enzymes like matrix metalloproteinases and cathepsin B into carrier molecules such as polymeric materials, lipids and silica.

In the study of Liu et al. (2015), matrix metalloproteinases (MMPs) responsive drug delivery system based on mesoporous silica nanoparticles (MSNs) was designed for

targeting tumor microenvironment. First, surface of MSNs was decorated with a diblock peptide composed of a polycation cell penetrating peptide (CPP), GR_6, and a matrix metalloproteinase 2 (MMP-2) substrate peptide, PVGLIGG. Then, DOX was loaded and finally, phenylboronic acid conjugated human serum albumin (PBA-HSA) was grafted onto the peptide functionalized MSNs to form MSNs-HSA-PBA@DOX. At the end of 24 h, only 15% of DOX was released from MSNs-HSA-PBA@DOX in the absence of MMP-2 whereas addition of MMP-2 increased % DOX release to 73 %. Cytotoxicity of MSNs, MSNs-HSA-PBA@DOX and free DOX was investigated using HepG2 cells. MSNs were found to be cytocompatible. Compared to free DOX, higher cell viability was obtained for MSNs-HSA-PBA@DOX with concentration dependent cytotoxicity. In vivo studies indicated tumor volumes of mice treated with MSNs-DOX nanoparticles were smaller than those of free DOX. Higher in vivo tumor treatment efficiency associated with lower side effects suggest that this enzyme responsive system has a value in cancer therapy (Y. Liu et al., 2015).

In another study, enzyme responsive multistage targeted DDS based on mesoporous silica nanoparticles (MSNs) was developed. MSNs were grafted with triphenylphosphine (TPP) and hyaluronic acid (HA) for targeting respective mitochondria and CD44 receptors, which was reported to be overexpressed in many cancer cells. DOX was loaded to the pores of MSNs to yield a composite carrier system denoted as MSN-DPH. Average sizes of MSNs and MSN-DPH were obtained as 50 nm and 110 nm, respectively. DOX release profiles of MSN-DOX and MSN-DPH in PBS (pH 7.4) were determined and are given in Figure 2.8. Fast release of DOX was obtained from MSN-

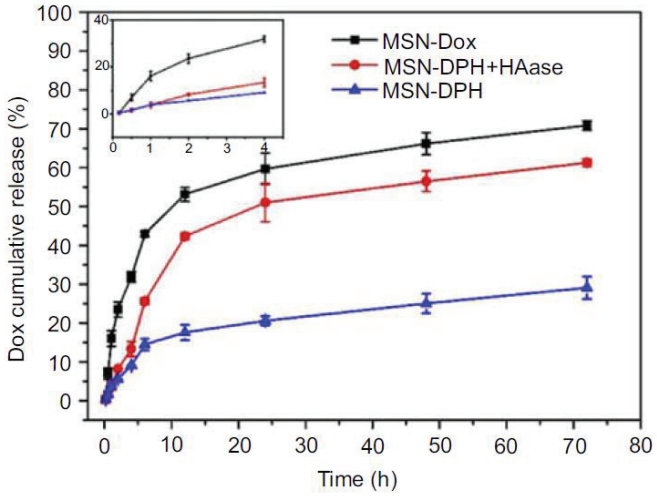

Figure 2.8. DOX release profiles of MSN-DOX, MSN-DPH and MSN-DPH in the presence of HAase (Naz et al., 2019)

DOX within 72 h. In the absence of hyaluronidase (HAase), slow release of DOX from MSN-DPH was observed indicating the capping effect of HA but after the addition of HAase, the release of DOX accelerated. Cytotoxicity of MSN and MSN-DPH nanoparticles was evaluated using Cos-7 (normal cells) and MGC-803 (cancer cells) cell lines. No cytotoxicity of MSN was observed against both cells. When normal cells were incubated with MSN-DPH, higher than 70% cell viability was obtained. However, MSN-DPH exhibited much higher cytotoxicity to cancer cells and enhanced antitumor effect of MSN-DPH was explained by the accelerated DOX release in MGC-803 cells containing HAase (Naz et al., 2019).

Recently, Şentürk and Top (2018) have developed PEG-peptide-DOX conjugates containing cathepsin B degradable sequence. Some of the examples of other enzyme-degradable drug delivery systems including HPMA-based copolymers with a GFLG linker and human serum albumin-DOX conjugate linked by cathepsin B degradable RRALAL sequence can be found in the introduction part of this reference (Şentürk and Top, 2018).

2.4. Drug Delivery Systems Containing Endosome Disruptive Units

Molecules with endosome disruptive property have been mostly incorporated to DNA or siRNA delivery systems. However, they were also shown to be used to cope with MDR effect of cancer cells. In one of such studies, Li et al. (2013), developed novel lipid-nanoparticle assemblies (LNPs) consisting of DOX conjugated dimethyldidodecylammonium bromide (DMAB) modified poly (lactic-co-glycolic acid) (PLGA) capped with 1,2-dipalmitoyl-sn-glycero-3-phosphocholine (DPPC) shell. DOX-PLGA nanoparticles were prepared by emulsification-diffusion method. The lipid, DPCC, was used to enhance endosome disruptive ability of the polymer. Average particle sizes of polymeric nanoparticles and LNPs were obtained as 180 nm and 210 nm, respectively. 32.5 % DOX was released during 72 h at pH 7.4. The slightly higher amount of DOX release from LNPs was observed in acidic environments (pH 5.5 and pH 6.5). Cytotoxicity tests performed using DOX resistant MCF-7/ADR and HK-60/ADR cell lines indicated that IC50 values of DOX conjugated LNPs was much lower than those of free DOX (Figure 2.9). Thus, this study confirmed that multidrug resistance could be

overcome by incorporating endosome disruptive units into the drug carrier systems (Li et al., 2013).

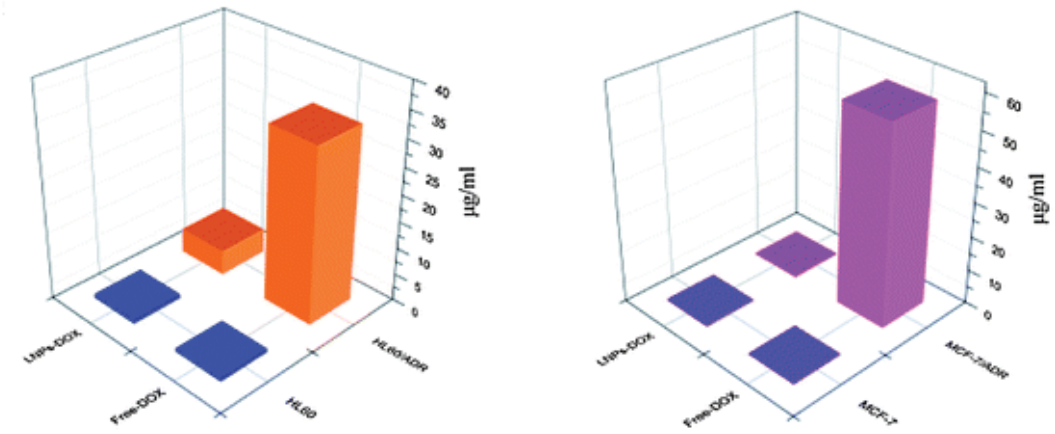

Figure 2.9. IC50 values of free DOX and of LNPs developed by Li et al. (2013)

2.5. PEG-Peptide Drug Delivery Systems

Recently, PEG-peptide-DOX systems with pH and enzyme responsive properties were prepared by our research group. In the study of Şentürk and Top (2018), methoxy polyethyelene glycol (mPEG) and peptide (AT3, $CG_3H_6R_2ALALG_3E$) containing drug delivery system was developed and DOX was conjugated to the carrier system via stable amide linkage to yield mPEG-AT3-DOX. pH responsiveness of the DDS was expected to be imparted by histidines and cathepsin B enzyme degradation was provided by R_2ALAL sequence. The particle size values were obtained as 15-30 nm and 15-20 nm for mPEG-AT3-DOX and mPEG-DOX, lacking peptide domain, respectively. DOX release profiles of mPEG-DOX and mPEG-AT3-DOX at different pH values and in the presence of cathepsin B are given in Figure 2.10. Maximum amount of DOX release was obtained in the presence of cathepsin enzyme as 17 ± 2 % for mPEG-AT3-DOX whereas in absence of the enzyme, % drug release of this system was obtained as 8.5 ± 3 % at acidic pH. Cytotoxicity of DDSs was evaluated using A549 and PC3 cell lines. IC50 values indicated that mPEG-AT3-DOX and free DOX showed similar cytotoxicity which was slightly higher than that of mPEG-DOX for both cell lines. Interestingly, AT3 and mPEG-

AT3 had also exhibited some noticeable degree of cytotoxicity against PC3 than A549 cells. It was proposed that PEG-peptide-DOX conjugate developed in this study could be used for cancer therapy if pH responsive behavior of the drug delivery system could be improved, possibly by increasing the number of histidines (Şentürk & Top, 2018).

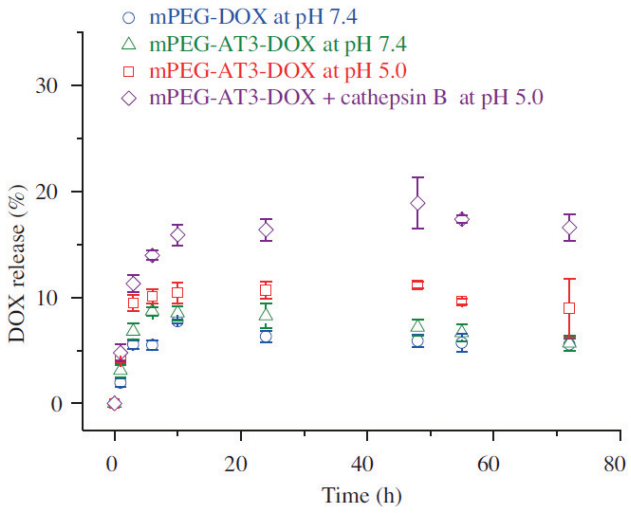

Figure 2.10. DOX release profiles of the mPEG-amide-DOX and mPEG-AT3-amide-DOX conjugates developed by Şentürk & Top (2018)

In a similar study, mPEG-peptide-DOX and mPEG-DOX (control group) drug delivery systems were developed (Balcı & Top, 2018). Different from the study of Şentürk and Top (2018), DOX was conjugated to the carrier molecules by using acid cleavable hydrazone linkage. Peptide sequence was designed as $CG_3H_6G_3E$ and pH responsiveness was obtained by using histidines. At pH 7.4, average sizes of the self-assembled conjugates were obtained as 9 ± 0.5 and 12 ± 2 nm for the control group and mPEG-peptide-DOX, respectively. DOX release profiles of mPEG-DOX and mPEG-peptide-DOX at neutral and acidic pH are given in Figure 2.11. mPEG-peptide-DOX showed slightly higher pH responsiveness than mPEG-DOX, which was attributed to the presence of histidines in the peptide sequence. Cytotoxicity was tested using A549 cell lines and IC50 values of free DOX, mPEG-DOX and mPEG-peptide-DOX were obtained as 0.96 ± 0.51, 21.9 ± 5.9 and 5.55 ± 0.75 μg/mL, respectively. (Balcı & Top, 2018).

These studies indicated DDSs based on PEG and peptides could have a value in cancer therapy not only for their simple design but also the possibility of incorporating biologically active motifs to the carrier systems. In this thesis, a peptide sequence with

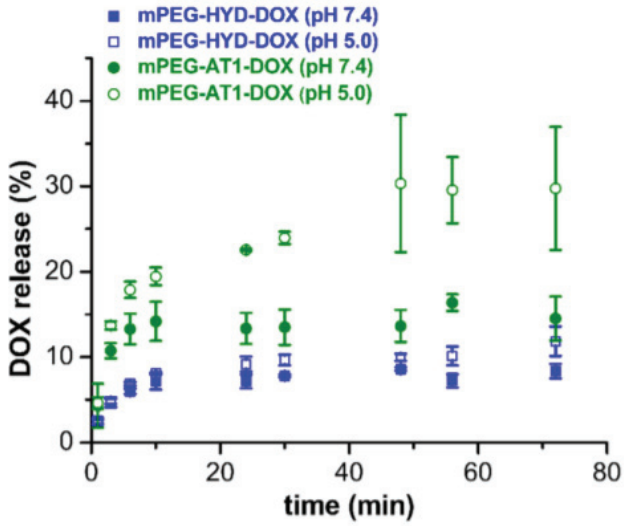

Figure 2.11. DOX release profiles of mPEG-hydrazone-DOX and mPEG-AT1-hydrazone-DOX developed by Balcı & Top (2018)

endosome disruption ability (TAT derived peptide) was used to overcome multidrug resistance of cancer cells. Additionally, different from its predecessors, another pH cleavable linkage, oxime bond, was used in this thesis.

CHAPTER 3

MATERIALS AND METHODS

3.1. Materials

Polyethylene glycol monomethylether (mPEG-OH, MW:1900 Da, Alfa Aesar) was used to prepare functionalized forms of methoxy-polyethylene glycol. Molecular sieves (zeolite 4Å beads), chromium oxide (CrO_3), acetone, isopropyl alcohol, diethyl ether (DEE) dimethyl sulfoxide (DMSO), dichloromethane (DCM), triethylamine (TEA) and acetic anhydride purchased from Sigma Aldrich were used in these functionalization reactions. Doxorubicin.HCl (DOX, Medkoo Biosciences) was used as a model anticancer drug. Sephadex LH-20 resin utilized in the gel permeation chromatography was obtained from GE Healthcare.

For the solid phase peptide synthesis (SPPS), low loading rink amide MBHA resin (NovaBiochem), dimethyl formamide (DMF, Sigma-Aldrich) and piperidine (Acros) were used. N, N-diisopropylethylamine (DIEA), 1-[bis(dimethylamino)methylene]-1H-1,2,3-triazolo[4,5-b] pyridinium 3-oxid hexafluorophosphate (HATU), O-(1H-6-chlorobenzotriazole-1-yl)-1,1,3,3-tetramethyluronium hexafluorophosphate (HCTU), and Fmoc-L-Gln(Trt)-OH, were purchased from Carl Roth. Other protected aminoacids used were Boc-L-Gly-OH, (Sigma-Aldrich) and Fmoc-Ser(tBu)-OH (Aldrich), Fmoc-L-Gly-OH, and Fmoc-L-Arg(Pbf)-OH, (NovaBiochem). In the peptide cleavage and deprotection reactions, synthesis grade trifluoroacetic acid (TFA, Sigma-Aldrich), anisole, thioanisole (Carl Roth) and 1,2-ethanedithiol (EDT, Fluka) were used.

For the preparation of the buffers, sodium phosphate monobasic, sodium phosphate dibasic, sodium chloride, sodium hydroxide (Sigma-Aldrich), acetic acid and hydrochloric acid (Merck) were used.

Sinapic acid, FTIR grade potassium bromide (Sigma Aldrich), deuterated chloroform ($CDCl_3$, Merck) were used for the sample preparation in respective MALDI-TOF mass spectroscopy, FTIR and NMR spectroscopy experiments. Spectroscopic grade

trifluoroacetic acid (Sigma-Aldrich) and acetonitrile (Isolab) were employed in HPLC analyses.

All chemicals and solvents were used with any purification. Deionized water was used in the preparation of aqueous solutions.

3.2. Synthesis of Methoxypolyethylene Glycol – oxime – Doxorubicin (mPEG-oxime-DOX) Conjugate

mPEG-oxime-DOX conjugate was synthesized by following two steps. First, methoxypolyethylene glycol (mPEG-OH) was oxidized to methoxypolyethylene glycol aldehyde (mPEG-COH) by using Albright-Goldman oxidation reaction. Then, the model anticancer drug, DOX, was conjugated to mPEG aldehyde by Schiff base formation between amine group of DOX and aldehyde group of mPEG.

3.2.1. Synthesis of Aldehyde Functionalized mPEG (mPEG-COH)

Aldehyde functionalized mPEG was synthesized by using DMSO-acetic anhydride oxidation via three different methods adapted from Harris et al. (1984) and Lin et. al. (1994). All the methods are based on Albright-Goldman oxidation and their common reaction schema is given in Figure 3.1. Details of the methods are summarized in Table 3.1. In the first method, suggested by Harris et al. (1984), the reaction was carried out without drying DMSO, mPEG-OH and glassware. In a typical reaction, mPEG-2000 (2.0 g, ~1.05 mmol) was dissolved in 6 mL DMSO and 0.252 mL (2.66 mmol) acetic anhydride was added. The mixture was stirred at room temperature for 30 h. After the reaction was completed, the solution was precipitated over cold DEE (stored at -20^{o}C) and centrifuged. The precipitate (mainly mPEG-COH and unreacted mPEG-OH) was dissolved in DCM reprecipitated on DEE and centrifuged twice. Finally, the isolated precipitate was dried in a vacuum oven at room temperature and stored at -20^{o}C (Harris et al., 1984; Y. S. Lin et al., 1994).

In the second method, same amounts of DMSO and acetic anhydride were used and the same procedure was applied as in the first method but the reaction was carried out under anhydrous conditions. All the glassware was dried at 125°C for at least 6 h. Moisture content of mPEG-OH was decreased in a vacuum oven overnight prior to the reaction. Zeolite 4Å was activated at 325°C for at least 16 h in a furnace and 50 mL DMSO was dried over the 5 g activated zeolite for 24 h and the drying procedure was repeated twice.

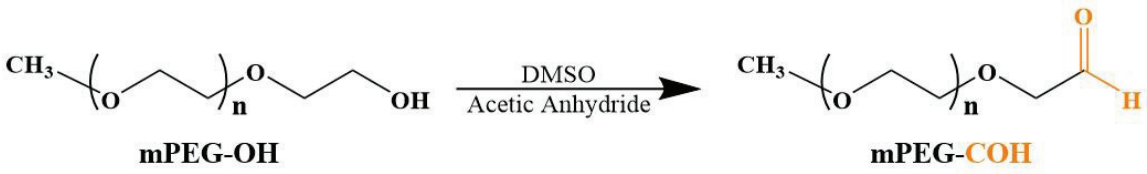

Figure 3.1. Synthesis of aldehyde functionalized mPEG

The third method was also carried out under anhydrous conditions but the amounts of DMSO and acetic anhydride were used according to the procedure applied by Lin et. al. (1994) and are given in Table 3.1. Drying conditions, reaction time, and isolation method followed in the third method were the same as in the other two methods applied in this study.

The products were obtained as white powder. Yields of mPEG-COH, mPEG-COH-D6 and m PEG-COH-D8 were obtained as 75%, 84% and 74%, respectively.

Table 3.1. Details of the mPEG-COH synthesis methods

Sample Code	Method number	Reaction conditions	DMSO (mL)	Acetic anhydride (mL)
mPEG-COH	1	Standard	6.00	0.252
mPEG-COH-D6	2	Anhydrous	6.00	0.252
mPEG-COH-D8	3	Anhydrous	8.82	0.218

3.2.2. Conjugation of DOX to mPEG-COH

Doxorubicin was conjugated to mPEG-COH via oxime bond that formed as a result of the reaction between amine group of DOX and aldehyde group of mPEG-COH as shown in Figure 3.2. DOX conjugation was performed using mPEG-COH-D8 sample by applying two methods, given with the details in Table 3.2.

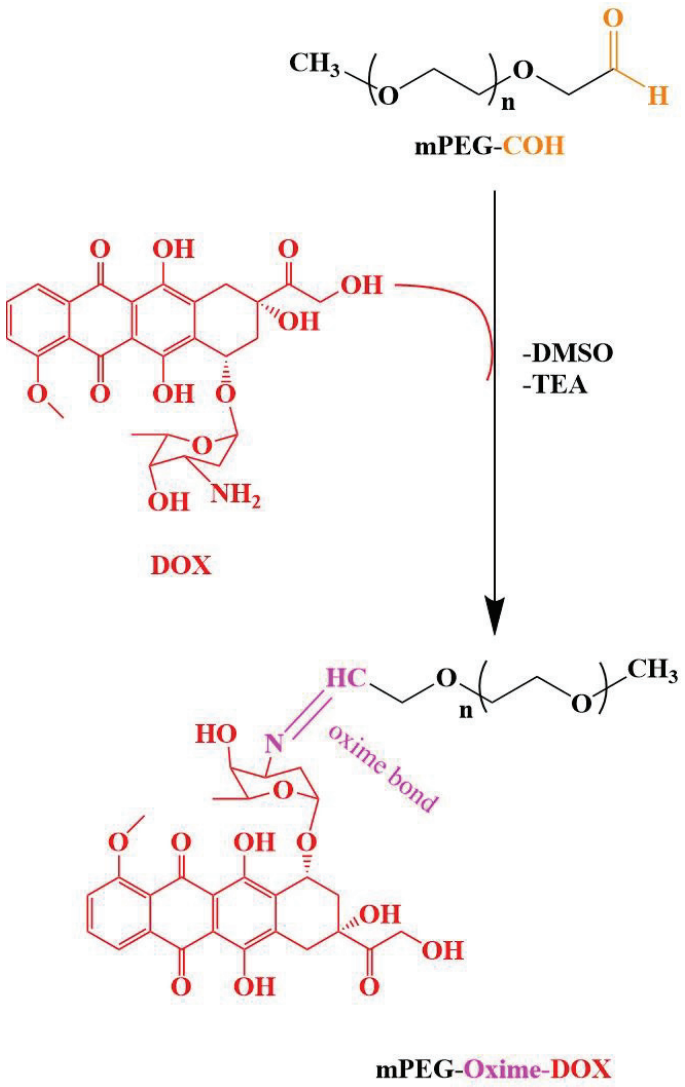

Figure 3.2. Reaction for the synthesis of mPEG-oxime-DOX conjugate

In the first method, the procedure similar to the one applied in Zhang et al. (2016) was used. In this reaction, 20 mg mPEG-COH (0.0105 mmol) and 6.5 mg DOX (0.011 mmol) were dissolved in 2 mL DMSO and 2.1 μL TEA was added. The solution was

shaken at 40ºC and 150 rpm for 24 h. Next, the reaction mixture was precipitated on cold DEE (stored at -20ºC) and centrifuged to isolate mPEG derivatives (Zhang et al., 2016). Then, the precipitate was washed with DEE and centrifuged until colorless washing solution was obtained. Residual DEE in the mPEG-oxime-DOX conjugate was evaporated in a fume hood. After that, gel permeation chromatography column was used to remove unreacted DOX as much as possible. The sample was dissolved in 1 mL DMSO and applied to a column containing Sephadex LH-20 resin suspended in DMSO, which was also used to elute the samples from the column. After the fractions (0.5 mL) were collected, a colorimetric mPEG detection test based on barium chloride and iodine solution was used to distinguish the fractions containing mPEG derivatives. For this test, 5% (w/v) barium chloride ($BaCl_2$) solution was prepared in 1 M hydrochloric acid and 0.127 g iodine was dissolved in 10 mL 2% (w/v) potassium iodine. 40 µL sample (4 µL of the fraction eluted and 36 µL deionized water) was mixed with 10 µL $BaCl_2$ solution and 5 µL iodine solution. The fractions containing mPEG derivatives were identified by brown color whereas the control sample prepared in the absence of mPEG (mixture of 40 µL deionized water, 10 µL $BaCl_2$ and 5 µL iodine solution) gave yellowish color (Gong et al., 2007). In the second method, the same procedure as the first method was followed except the amount of DOX and TEA was increased as given in Table 3.2.

Table 3.2. Reaction conditions of mPEG-oxime-DOX conjugate synthesis methods

Sample Code	Method number	Amount of DOX (mg)	Amount of TEA (µl)	DMSO (mL)
mPEG-oxime-DOX-1	1	6.50	2.10	2.00
mPEG-oxime-DOX-2	2	8.70	6.30	2.00

The fractions containing mPEG derivatives were collected and precipitated on ice cold DEE. Next, DEE was removed in the fume hood and the conjugates were dissolved in deionized water. Then, they were freeze dried and stored at -20ºC. The yields were obtained as ~70% and ~80% for the samples mPEG-oxime-DOX-1 and mPEG-oxime-DOX-2, respectively.

3.3. Synthesis of mPEG-Peptide-oxime-DOX Conjugate

mPEG-peptide-DOX conjugation was synthesized by employing the following steps given below:

- Preparation of carboxylic acid functionalized mPEG (mPEG-COOH) using Jone's oxidation
- Solid phase peptide synthesis and conjugation of mPEG-COOH to the peptide on the resin to obtain mPEG-peptide with hydroxyl functionality (mPEG-peptide-OH)
- Synthesis of aldehyde form of the mPEG-peptide conjugate (mPEG-peptide-COH) using Albright-Goldman oxidation
- Obtention of mPEG-oxime-DOX via conjugation of DOX to mPEG-peptide-COH by using amine-aldehyde reaction

3.3.1 Synthesis of Carboxylic Acid Functionalized mPEG (mPEG-COOH)

Carboxylic acid functionalized mPEG (mPEG-COOH) was prepared by using the procedure developed by Lele & Kulkarni (1998) based on Jone's oxidation reaction given in Figure 3.3. First, the oxidizing agent, Jone's reagent, was prepared by dissolving 7 g (0.07 mol) chromium trioxide (CrO_3) in 50 mL deionized water. 6.1 mL H_2SO_4 was added in small portions to the mixture while stirred on an ice-water bath for additional 10 min and the mixture was allowed to reach to the room temperature prior to the use (Lele & Kulkarni, 1998).

In a typical oxidation reaction, 5 g mPEG-OH (~ 0.0025 mol) was dissolved in 50 mL acetone and 2.125 mL of Jone's reagent was added to this solution. After the addition of Jone's reagent, brownish color was observed first, and then, in a few minutes, the color changed to green/blue-green indicating the formation of chromium salts. The mixture was stirred overnight at room temperature. Finally, 1.25 mL isopropyl alcohol was added to quench the reaction. To isolate oxidized mPEG, chromium salt precipitates

were filtered. Next, 0.5 g activated carbon was added to filtered solution to adsorb remaining chromium salts and the mixture was stirred for 2 h. After that, activated carbon was syringe filtered and adsorption procedure was repeated until colorless solution was obtained. Acetone in the clear solution was evaporated by a rotary evaporator and the polymer was allowed to solidify in petri dishes incubated at 37°C. Finally, residual solvent in the solidified product was removed by vacuum at 40°C.

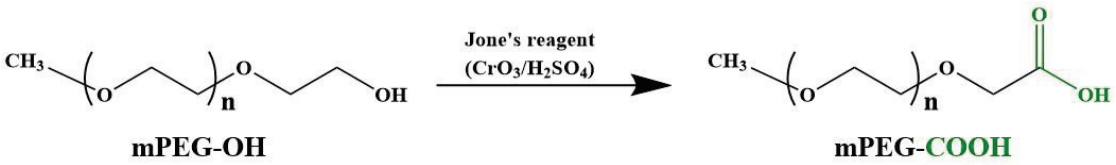

Figure 3.3. Synthesis of carboxylic acid functionalized mPEG

The product, carboxylic acid functionalized mPEG, was obtained as white powder. Yield of the product was obtained as 64.4%.

3.3.2. Solid Phase Synthesis of the Peptide and mPEG-peptide Conjugate

The peptide with a sequence of $G_2RQR_3QR_3G_2S$ was synthesized by employing Fmoc strategy in the solid phase peptide synthesis (SPPS). The reaction was carried out using AAPTEC Focus XI model automated peptide synthesis instrument.

0.572 g (0.2 mmol) rink amide resin was used. DMF-DMSO mixture at 1:1 volume ratio was used for swelling and washing the resin after the deprotection and coupling reactions as well as for dissolving the reagents used in these reactions. Deprotection reactions was carried out by contacting the resin with 20% (v/v) piperidine solution. In order to reduce the number of functional groups of the resin (resin loading), mixture of Boc-L-Gly-OH (0.5 mmol), and Fmoc-Ser(tBu)-OH (0.3 mmol) was used in the first two coupling reactions. In this set of coupling reactions, 0.79 mmol coupling agent was used along with 2 mmol DIEA. For the rest of amino acid coupling reactions, the amounts of coupling agents, amino acids and DIEA were halved. Double coupling

was applied for each amino acid and HCTU and HATU were employed in the first and the second coupling reactions, respectively. After the addition of the amino acids was completed, approximately one quarter of the resin was saved for the analysis. PEGylation of the peptide was carried out by coupling 0.5 mmol of mPEG-COOH to the N-terminus of the peptide on the resin with the aid of 0.395 mmol HATU and 1 mmol DIEA for extended reaction periods, i.e. 6 h for the first coupling reaction and 12 h for the second coupling reaction. After the synthesis, the resin was washed with DCM and dried in a vacuum oven at room temperature. Cleavage and deprotection reactions were performed by contacting the resin with a cocktail containing 90% TFA, 5% thioanisole, 3% EDT and 2% anisole for 3.5 h. 20 ml cleavage cocktail was used for 1 g of the resin. Then, the resin was filtered and the supernatant was precipitated on cold DEE stored at -20^{o}C. The precipitate was washed with DEE and centrifuged three times. DEE in the isolated peptide/conjugate was evaporated under N_2 flow at room temperature and then, the products were dissolved in deionized water, freeze dried, and were stored at -20^{o}C.

3.3.3. Synthesis of DOX-conjugated mPEG-peptide

Aldehyde functionalized mPEG-peptide was synthesized by DMSO-acetic anhydride oxidation similar to the method 3 given in Section 3.2.1 under anhydrous conditions. Hydroxyl group of serine was oxidized to aldehyde as given in Figure 3.4. For this reaction, 30 mg vacuum dried mPEG- peptide (0.00815 mmol) was dissolved in 2 mL dried DMSO and 2 μL (0.0188 mmol) acetic anhydride was added. The mixture was stirred at room temperature during 30 h. Then, it was precipitated on cold DEE and centrifuged. The precipitate was dissolved in DCM, reprecipitated on DEE and centrifuged twice. Finally, the product was dried in a vacuum oven and stored at -20^{o}C. The reaction yield was obtained as ~76%.

DOX was conjugated to aldehyde group of the conjugate via Schiff base formation. The reaction schema is given in Figure 3.5. Approximately, 9 mg mPEG-peptide-COH and 2.5 mg DOX were dissolved in 1 mL DMSO and 22 μL TEA was added. The method explained in Section 3.2.2 was followed to synthesize mPEG–peptide–oxime-DOX conjugate.

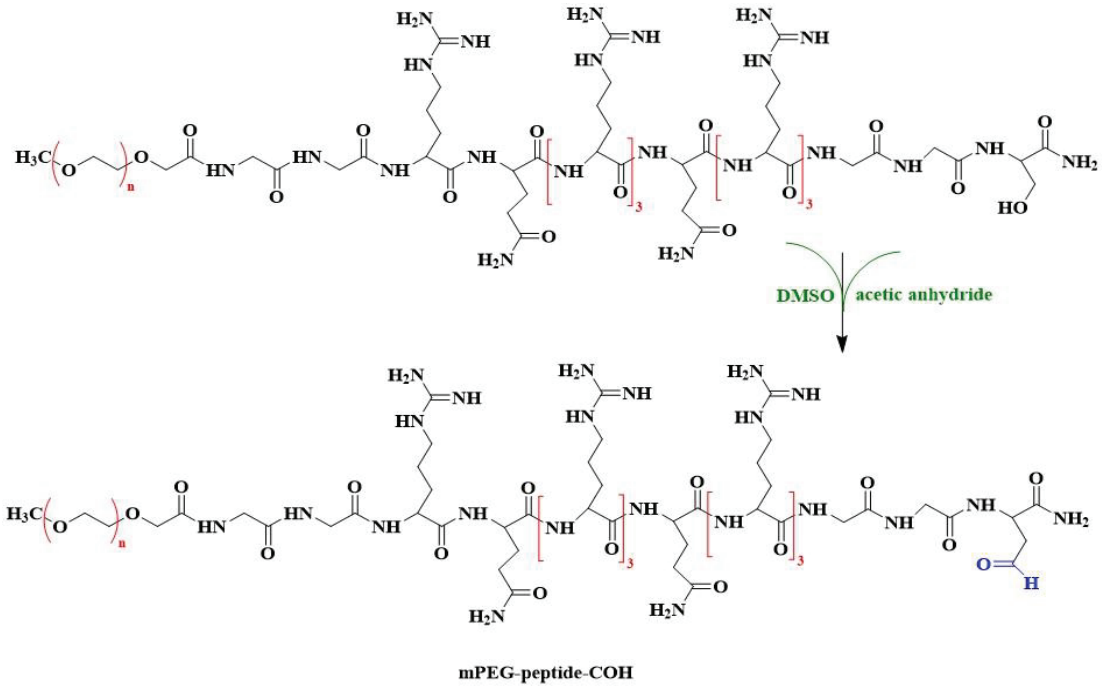

Figure 3.4. Synthesis of aldehyde functionalized mPEG-peptide (mPEG-peptide-COH)

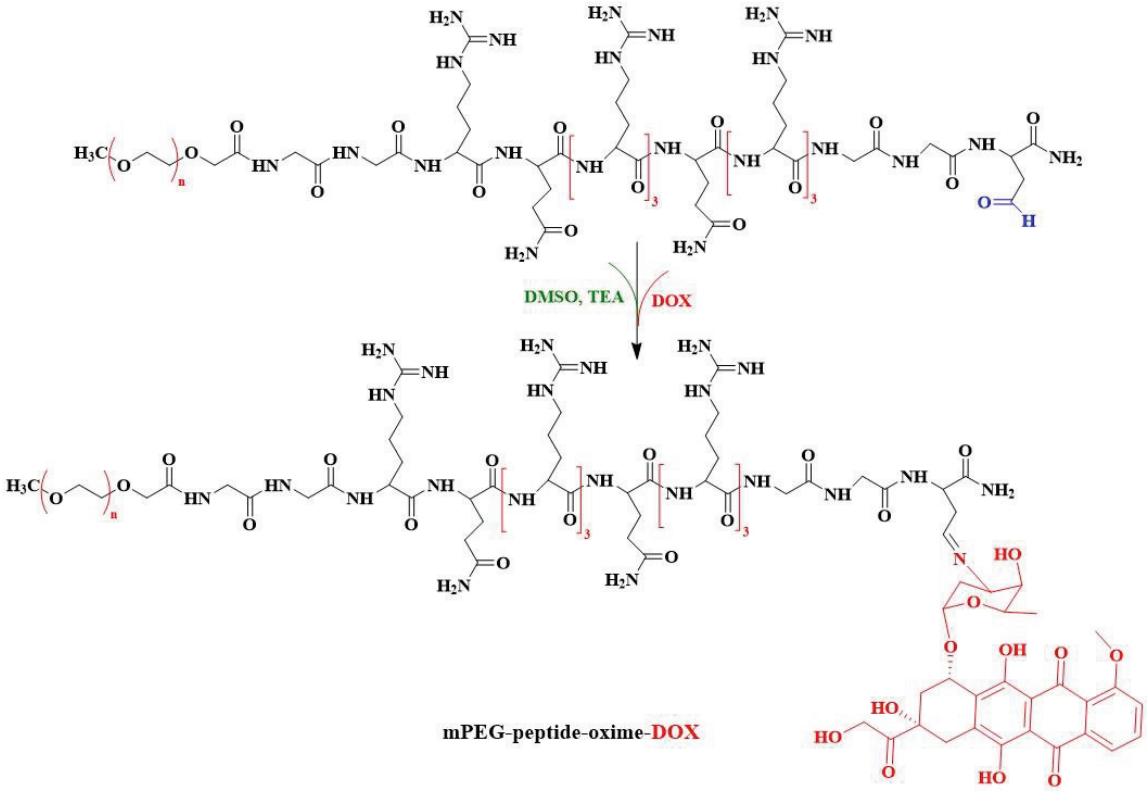

Figure 3.5. Reaction schema of DOX conjugation to mPEG-peptide-COH

3.4. Spectroscopic Analyses

Functional groups of the drug carrier systems were determined using Fourier Transform Infrared Spectroscopy (FTIR) analysis. FTIR experiments were performed by using KBr pellet technique on a Shimadzu IR Prestige-21 FTIR-8400S model spectrophotometer. Prior to analyses, moisture of samples was removed in a vacuum oven at room temperature. Approximately 1.5 mg sample was dispersed in 150 mg of potassium bromide (KBr) to prepare pellets. The spectra were taken between 400 cm^{-1} and 4000 cm^{-1} wavenumbers.

1H Nuclear Magnetic Resonance (NMR) spectroscopy was used to quantify the functional groups of the functional mPEGs and molar masses of these polymers. Approximately, 10 mg sample was dissolved in 0.6 mL deuterated chloroform ($CDCl_3$) and was subjected to H-NMR analysis. The experiments were conducted by using a Varian Vnmr 400 model instrument. The data were analyzed with the aid of ACDLAB 12, 1D NMR Processor software.

Molar masses of the peptide and the mPEG-peptide conjugate were determined by using a Bruker Daltonics – Autoflex III Smartbeam model matrix-assisted laser desorption/ionization time of flight mass spectroscopy (MALDI-TOF-MS). These experiments were carried out at Biological Mass Spectrometry and Proteomics Facility of İzmir Institute of Technology located at the Department of Chemistry.

DOX contents of the conjugates were determined by using the extinction coefficient of adriamycinone, which was reported to be the hydrolysis product of doxorubicin. Approximately, 0.50 mg sample was dissolved in 800 µL 1 N HCl and hydrolyzed at 50ºC for 2 h. After cooling, 750 µL DMSO was added to 250 µL of the hydrolyzed sample. Then, absorbance of the solution was measured at 488 nm on a Shimadzu UV-2450 model UV-Vis spectrophotometer. % DOX content was calculated by using the following equations in which the molar absorbance coefficient was taken as 15551 $L.mol^{-1}.cm^{-1}$ based on the previously constructed calibration curve (Şentürk & Top, 2018).

$$\text{DOX content } \% = \frac{C_{\text{DOX measured}} \left(\frac{\text{mmol}}{\text{ml}}\right)}{C_{\text{conjugate}} \left(\frac{\text{mmol}}{\text{ml}}\right)} \times 100\%$$

$$C_{DOX\ measured}\ (\frac{mmol}{ml}) = \frac{\text{Absorbance measured at 488 nm}}{\text{Molar Absorbance Coefficient} \times \text{Path Length}}$$

$$C_{conjugate}\ (\frac{mmol}{ml}) = \frac{\text{Mass concentration of the conjugate } (\frac{mg}{ml})}{\text{Molar mass of the conjugate } (\frac{mmol}{mg})}$$

3.5. High Performance Liquid Chromatography (HPLC) Analyses

Purity of the peptide and mPEG-peptide conjugate was assessed by applying reverse phase HPLC analysis performed on an Agilent 1100 model HPLC system. 0.1% TFA in deionized water and 0.08% TFA in acetonitrile were used as solvent A and solvent B, respectively. 100 μL of filtered sample dissolved in solvent A (~ 1-2 mg/ml) was injected to a C18 analytical column (Inertsil WP-300, 5 μm, 4.6 × 100 mm). After the equilibration of the column with a solvent A: solvent B ratio of 95:5, the ratio was changed to 30:70 within 65 min. The samples were eluted with a solvent flowrate of 1 ml/min and the chromatograms were obtained by measuring the absorbance at 214 nm using a UV detector.

3.6. Size Distribution and Stability Analyses

Size distributions of the mPEG-oxime-DOX and the mPEG-peptide-oxime-DOX conjugates were determined by using dynamic light scattering technique on a Malvern ZetaSizer Nano ZS model instrument. Each sample was dissolved in deionized water at 2 mg/ml concentration and diluted twice with 20 mM acetate buffer and 300 mM NaCl at pH 5.0 (2 × acetate buffer) or 20 mM phosphate buffer and 300 mM NaCl (2 × PBS) at pH 7.4. Then, the solutions were filtered using a syringe filter with a pore size of 0.2 μm. Correlation functions were obtained at 25^{o}C for the as prepared sample, and after incubating the sample at 37^{o}C for 1 day. Time dependent size distributions, D10, D50, and D90 values of the samples were determined by taking average of three measurements based on CONTIN method provided by the instrument.

3.7. Drug Release Experiments

DOX release profiles of the samples were obtained by using dialysis method. 2 mg/ml of the samples were prepared in deionized water and diluted twice with 2 × acetate buffer at pH 5.0 or 2 × phosphate buffer (PBS) at pH 7.4. 0.5 ml of solution was placed in a dialysis membrane with MWCO of 3.5 kDa. The membrane was transferred to a glass vial containing 12.5 ml buffer (1 × acetate buffer at pH 5.0 or 1 × phosphate buffer (PBS) at pH 7.4). The solutions were incubated at 37°C by shaking at 150 rpm. At certain time intervals (1 h, 2 h, 3 h, 6 h, 24 h, 30 h, 48 h, 54 h), 105 µl of samples was withdrawn and replaced with the fresh buffer with equal volume. Two independent sets of experiments were performed for each sample.

DOX concentrations in the released media were determined by using calibration curves of free DOX in each buffer based on fluorescence measurements. Fluorescence emission measurements were performed on VarioSkan Flash Multimode Reader (Thermo Scientific) model microplate reader at 590 nm. Excitation wavelength was used as 480 nm. Free DOX concentrations were varied between 0.025-2 µg/ml for the construction of the calibration curves, which are given in Figure A.3 and Figure A.4 at pH 5.0 and 7.4, respectively. The equations used for the calculation of % DOX release are given below. A sample calculation is presented in Appendix B.

$$\%\ \text{DOX release} = \frac{C_t(\mu g\ \text{of DOX released at time t})}{C_i(\mu g\ \text{of DOX in the conjugate initially})} \times 100\ \%$$

$$C_t = \frac{\text{Fluorescence intensity at 590 nm}}{\text{Slope of calibration curve at 590 nm}} \times V_{dialysis}\ (\text{ml}) \times \text{Dilution factor}$$

$$C_i = \frac{C_{conjugate}\left(\frac{mg}{ml}\right) \times V_{conjugate\ in\ membrane}\ (\text{ml}) \times MW_{DOX}\left(\frac{mg}{mmol}\right)}{MW_{conjugate}\left(\frac{mg}{mmol}\right)} \times \frac{\text{DOX conjugation \%}}{100\%} \times \frac{1000\ \mu g}{1\ mg}$$

CHAPTER 4

RESULTS AND DISCUSSION

4.1. Characterization of Functional mPEGs

Aldehyde and carboxylic acid functionalized mPEGs were used in the preparation of mPEG-oxime-DOX and mPEG-peptide conjugates, respectively. In this section, FTIR, and NMR spectroscopy results of these functional mPEGs along with those of the parent mPEG-OH are given.

4.1.1. Aldehyde Functionalized mPEG

In this study, DOX was conjugated to the carrier molecules (mPEG or mPEG-peptide) via acid cleavable oxime bond to ensure fast release of the drug in the endosomal compartments. In order to assess the effect of the TAT-derivative endosomal-disruptive peptide on the performance of the resultant drug delivery system, in addition to mPEG-TAT derivative peptide-DOX conjugate, mPEG-DOX system was also synthesized. For this purpose, DOX was attached to aldehyde form mPEG via Schiff base formation and aldehyde functionalized mPEG was synthesized, beforehand.

Aldehyde form of mPEG was prepared by using Albright-Goldman oxidation of the hydroxyl group of mPEG. Three different synthesis procedures were tested to maximize aldehyde functionalization. Oxidized forms of the mPEGs obtained by the methods described in Section 3.2.1 were characterized by using FTIR and NMR spectroscopy. Figure 4.1 indicated FTIR spectra of the parent mPEG-OH molecule and its oxidized forms. In all spectra, characteristic poly(ethylene glycol) vibration bands were observed at 1242, 1280, 1342, 1468, 2889 cm^{-1} (C-H vibrations), 3450 cm^{-1} (OH stretching), and 1113 cm^{-1} (C-O-C vibrations). However, in the spectra of the oxidized

samples a new band at 1738 ± 1 cm^{-1} related to carbonyl stretching formed confirming the transformation of the hydroxyl groups of the mPEG to the oxidization products (Mauri et al., 2015; Zheng et al., 2010).

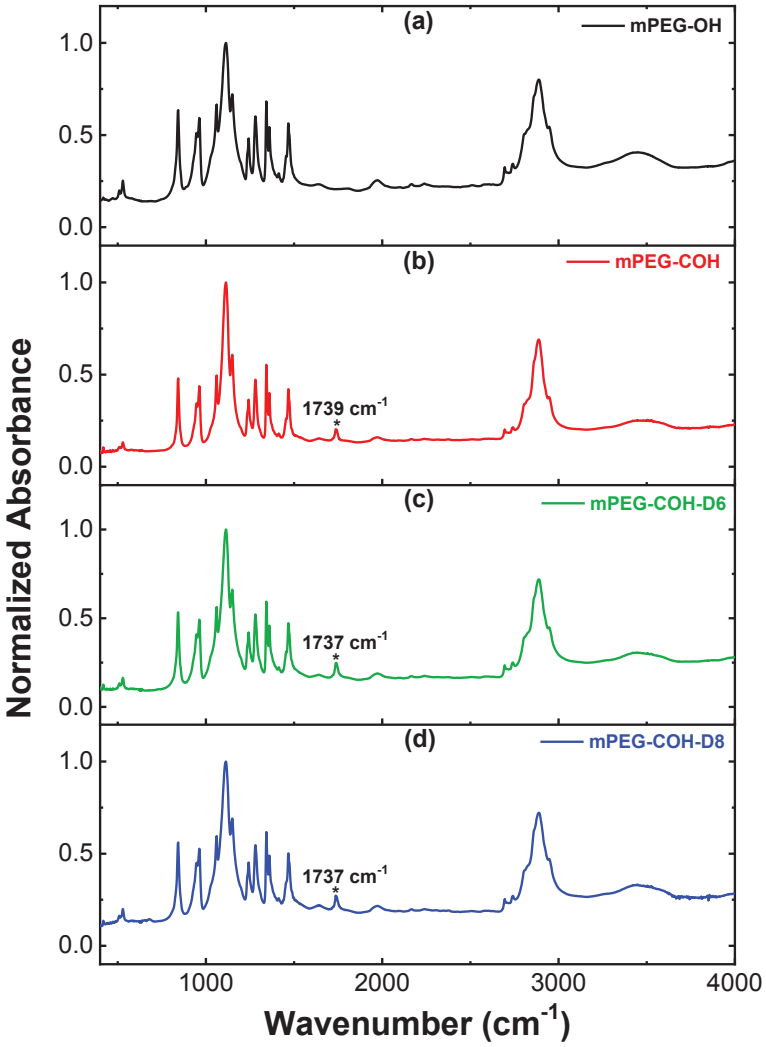

Figure 4.1. FTIR spectra of the a) mPEG-OH, b) mPEG-COH, c) mPEG-COH-D6 and d) mPEG-COH-D8

In order to qualify and quantify the aldehyde groups, 1H NMR analyses were conducted. The spectra of the samples, mPEG-OH, mPEG-COH, mPEG-COH-D6, and mPEG-COH-D8 are given in Figure 4.2, Figure 4.3, Figure 4.4 and Figure 4.5, respectively. Theoretical chemical shifts of the various functionalized mPEGs are given in Appendix in Figure A.3. Positions of the chemical shifts were calibrated according to the position of $CDCl_3$ solvent which appeared at 7.27 ppm. All spectra exhibited chemical shifts at about 3.65 ppm and 3.38 ppm. The large peak at 3.65 ppm is related to the protons

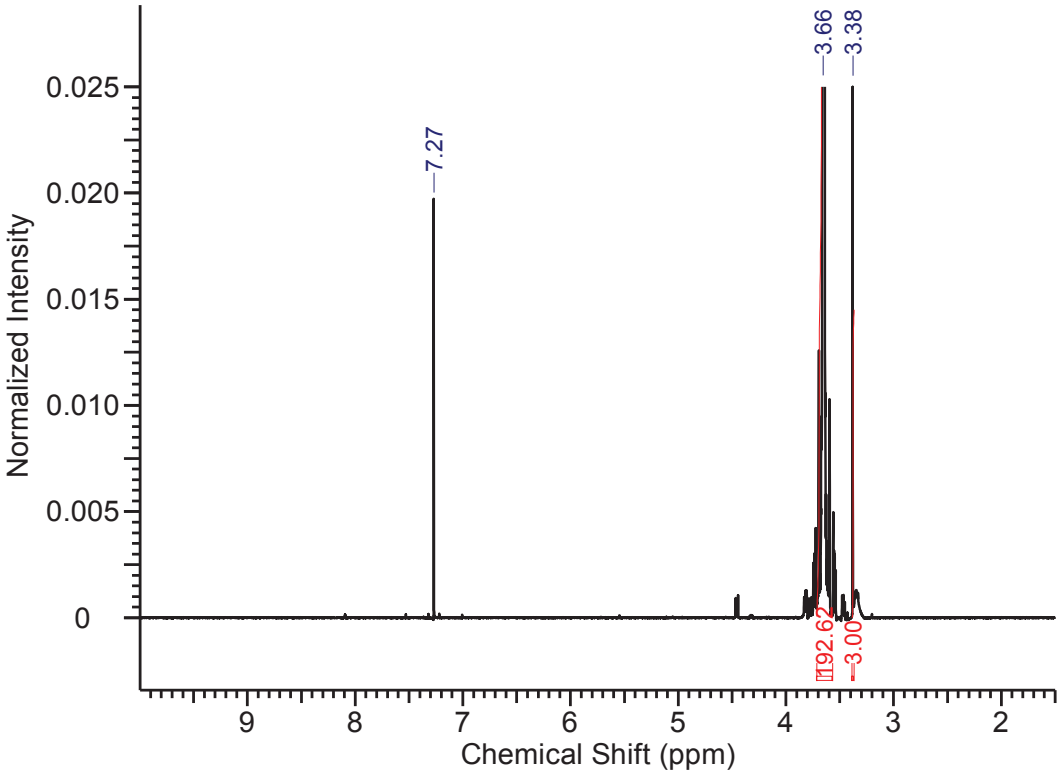

Figure 4.2. 1H NMR spectrum of the mPEG-OH in $CDCl_3$

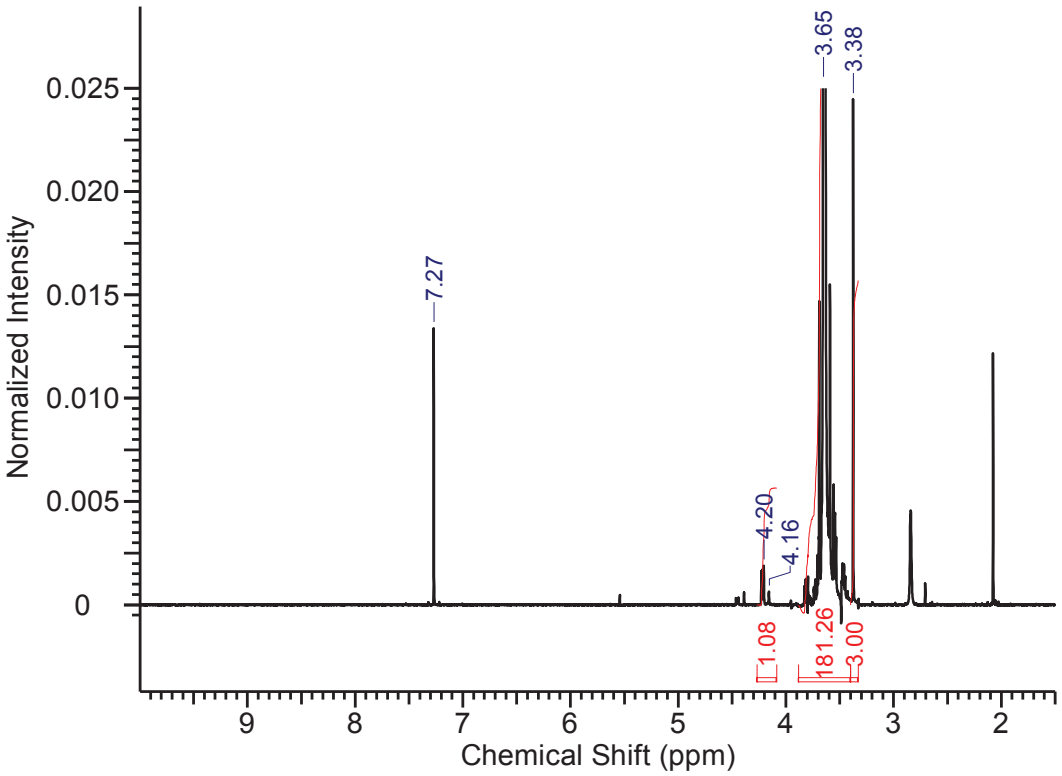

Figure 4.3. 1H NMR spectrum of the mPEG-COH in $CDCl_3$

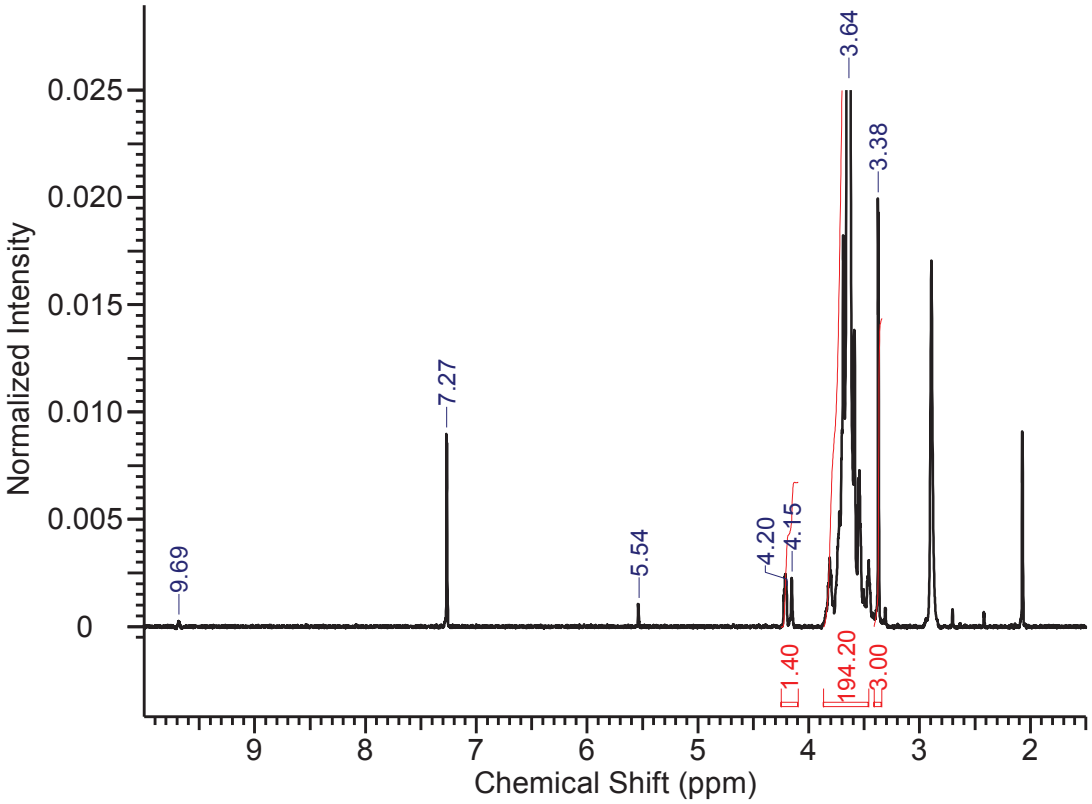

Figure 4.4. 1H NMR spectrum of the mPEG-COH-D6 in $CDCl_3$

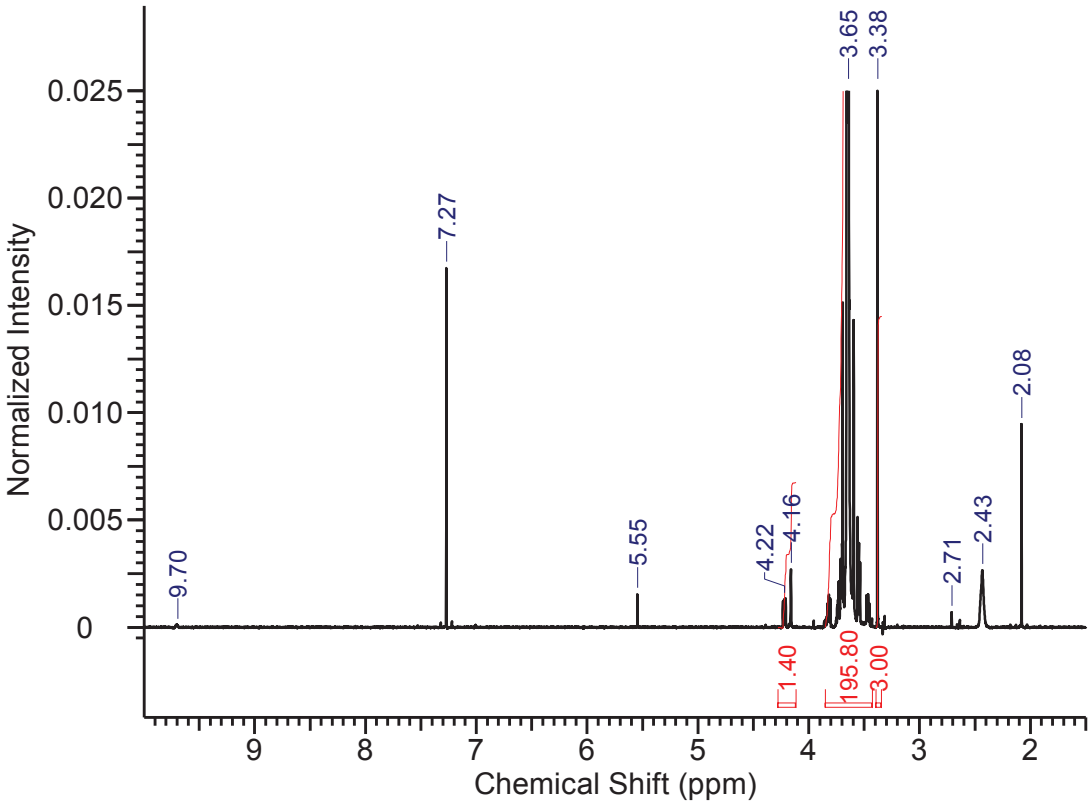

Figure 4.5. 1H NMR spectra of the mPEG-COH-D8 in $CDCl_3$

of the repeating unit whereas the peak at 3.38 ppm is due to 3 protons of the methoxy end group. By comparing the area of these two peaks, molar masses were obtained as 2120 Da, 1996 Da, 2139 Da, and 2156 Da for the samples mPEG-OH, mPEG-COH, mPEG-COH-D6, and mPEG-COH-D8, respectively indicating no significant change in molar mass during the oxidization reactions. It is noteworthy to mention that these molar masses agree with the molar mass specified by the supplier (1900 Da). Chemical shifts observed at 9.70 ppm confirmed the formation of aldehyde groups but the presence of the chemical shift related to hydroxyl protons observed at 5.55 ppm indicated oxidation process was incomplete for all the samples. Since aldehyde and hydroxyl protons can readily exchange with the deuteriums in the solvent, the peak areas of these protons can be misleading in quantitative analyses. For this reason, chemical shifts that appeared in all oxidized samples at 4.16-4.22 ppm related to the 2 protons attached to the carbon next to carbonyl group were used to quantify the aldehyde functionalization. By comparing the area of this newly formed protons (2 protons per chain) with the methoxy protons (3 protons per chain) % aldehyde functionalization values were obtained as 54%, 70%, and 70% for the samples mPEG-COH, mPEG-COH-D6, and mPEG-COH-D8, respectively. In addition to these peaks, a few peaks with chemical shifts below 3 ppm were also observed in the oxidized samples, which were likely due to some impurities that could not be removed. These peaks were also apparent in the NMR spectrum of a PEG-aldehyde sample synthesized using similar DMSO-acetic anhydride oxidation procedure (Zhang et al., 2016). Of the samples giving the highest aldehyde functionalization, mPEG-COH-D8 exhibited lower amount of impurities by taking account into their peak areas. For this reason, the method used to synthesize mPEG-COH-D8 was applied to the oxidation of the mPEG-peptide sample.

4.1.2. Carboxylic Acid Functionalized mPEG

Carboxylic acid functionalized mPEG (mPEG-COOH) was used in the solid phase PEGylation of the TAT-derived peptide and it was synthesized by using Jone's oxidation of the mPEG-OH. Figure 4.6 shows the comparison of FTIR spectra of the mPEG-OH and the mPEG-COOH. Characteristic PEG vibrations as given in section 4.1.1

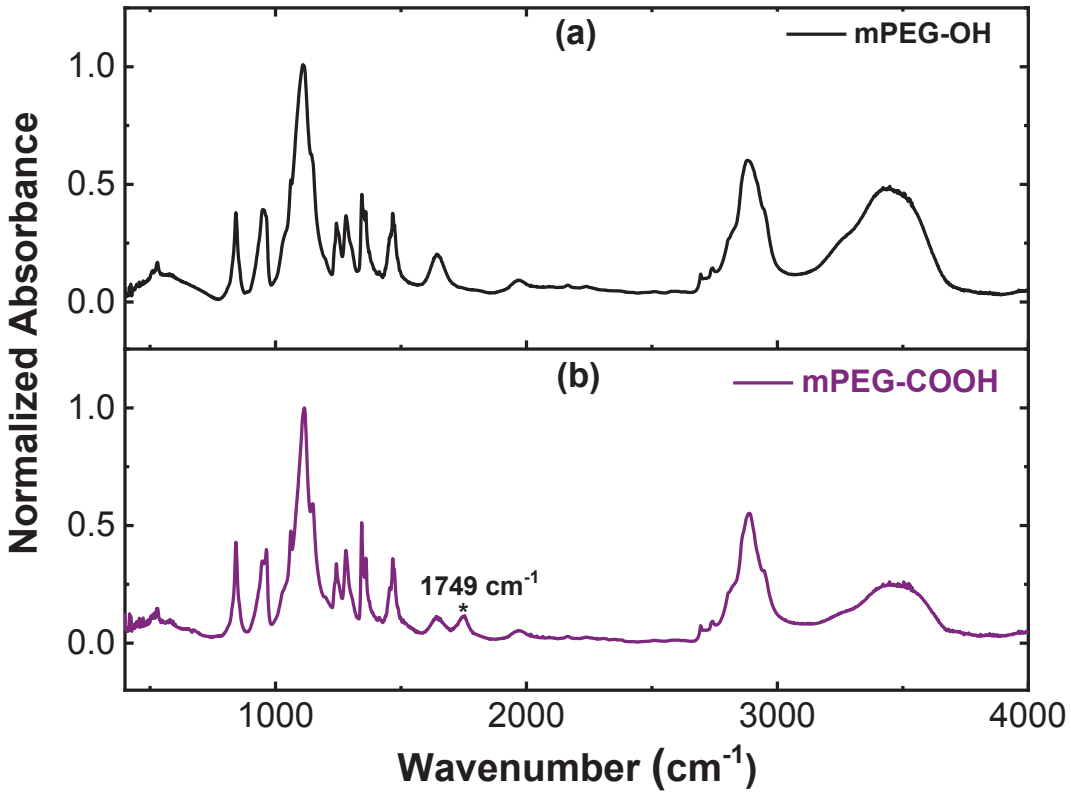

Figure 4.6. FTIR spectra of the a) mPEG-OH, and b) mPEG-COOH

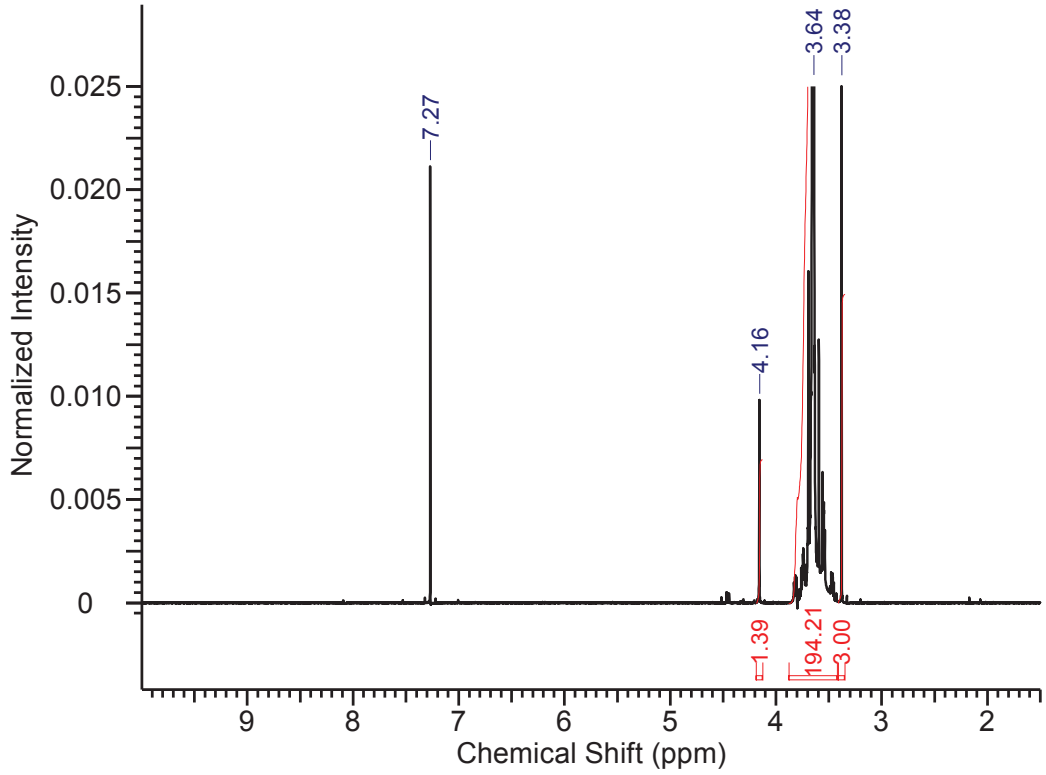

Figure 4.7. 1H NMR spectrum of the mPEG-COOH in $CDCl_3$

were observed in these spectra, as expected. However, there appeared a peak at 1749 cm^{-1} associated with carbonyl stretching of COOH groups in the spectrum of the mPEG-COOH confirming the oxidation reaction. 1H NMR spectrum of mPEG-COOH is given in Figure 4.7, and was used to estimate the degree of COOH functionalization. By comparing the area of the peak at 3.38 ppm due to methoxy (CH_3-O) groups and that of the peak at 3.66 ppm related to ether (O-CH_2-CH_2) backbone, number average molecular weight (M_n) of mPEG-COOH was calculated as 2191 Da, very close to the specified M_n value of the parent mPEG-OH molecule. The chemical shift at 4.16 ppm, appeared mPEG-COOH only, represented 2 protons attached to the carbon next to the carboxylic acid group. By comparing the area of this chemical shift with the area of methoxy protons, degree of carboxylic acid functional group was calculated as 69.5%, which seemed enough to use in the PEGylation reaction.

4.2. Characterization of the TAT-derived Peptide and mPEG-Peptide

The peptide with a sequence of $G_2RQR_3QR_3G_2S$ was used in this study. It was designed to provide both conjugation sites and endosome disruption property. In this peptide, serine was added to the sequence to attach DOX after oxidizing its hydroxyl group to aldehyde. The purpose behind the use of glycine residues at the N-terminus and before serine was to reduce steric hindrance during PEGylation and drug conjugation reactions.

TAT peptide fragments have been used in the design of gene or si-RNA delivery systems for their well-known endosome disruption ability (Tai & Gao, 2017). The original TAT (48-57) fragment, GRKKRRQRRR, contains two lysine residues, which could interfere the conjugation reactions followed. In order to make this sequence conjugation reaction compatible, KK residues were replaced by RR, QR, and RQ groups and the secondary structures of these sequences, estimated by PEPFOLD3 software were compared (Lamiable et al., 2016; Shen et al., 2014; Thevenet et al., 2012). The probability plots of the sequences $G_2RKKR_2QR_3G_2S$, $G_2R_5QR_3G_2S$, $G_2R_2QR_2QR_3G_2S$, and $G_2RQR_3QR_3G_2S$ are given in Figure A.2 in Appendix. In these plots, alpha helical, coil, and extended structures are represented by red, blue, and green color codes, respectively. Of the sequences tested, the one with slightly higher helicity $G_2RQR_3QR_3G_2S$ sequence

was selected, synthesized and PEGylated using solid phase synthesis procedure. The peptide and the mPEG-peptide conjugate were characterized by HPLC, FTIR, and MALDI-MS to confirm their purity.

Figure 4.8 indicates the HPLC traces of the mPEG-COOH, the peptide, and the mPEG-peptide conjugate. A single peak at 11 min was observed in the elution curve of the peptide indicating its high purity. mPEG-COOH was eluted between 19 min and 70 min appearing as a broad hump with three sharp peaks between 50 min and 55 min, which could be attributed to strong interaction of PEG chains with the column. In the chromatogram of mPEG-peptide, no significant amount of fraction corresponding to the peptide was observed confirming PEG conjugation was successful with a quite high yield. Thus, a number of peaks observed between 15 and 42 min could be attributed to the PEGylated peptide.

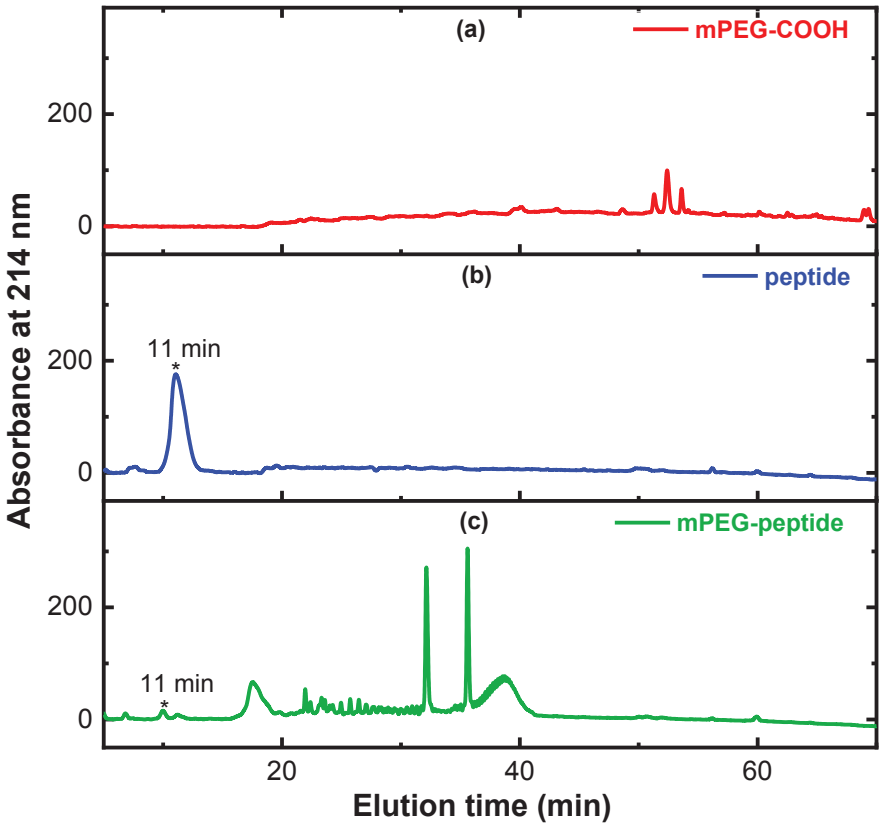

Figure 4.8. HPLC traces of the (a) mPEG-COOH, (b) peptide, and (c) mPEG-peptide

Comparison of FTIR spectra of the mPEG-COOH, the peptide, and the mPEG-peptide conjugate is given in Figure 4.9. In the spectrum of the mPEG-peptide the bands corresponding to characteristic PEG vibrations and amide bands of peptide were observed. For the peptide and the mPEG-peptide, amide I band was observed at

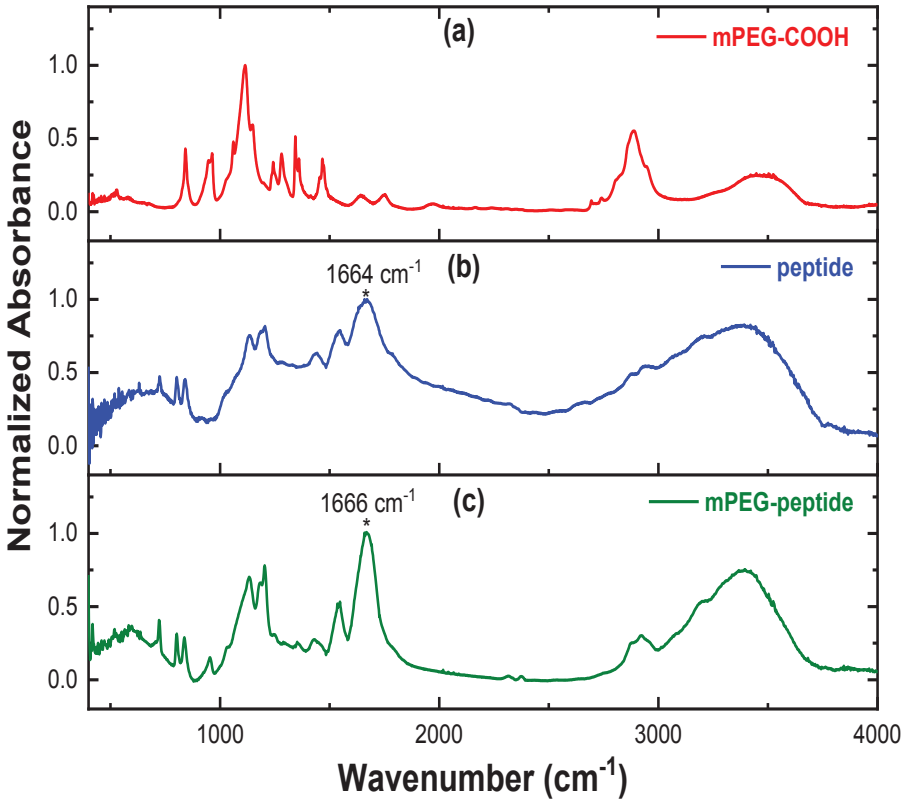

Figure 4.9. FTIR spectra of the (a) mPEG-COOH, (b) peptide, and (c) mPEG-peptide

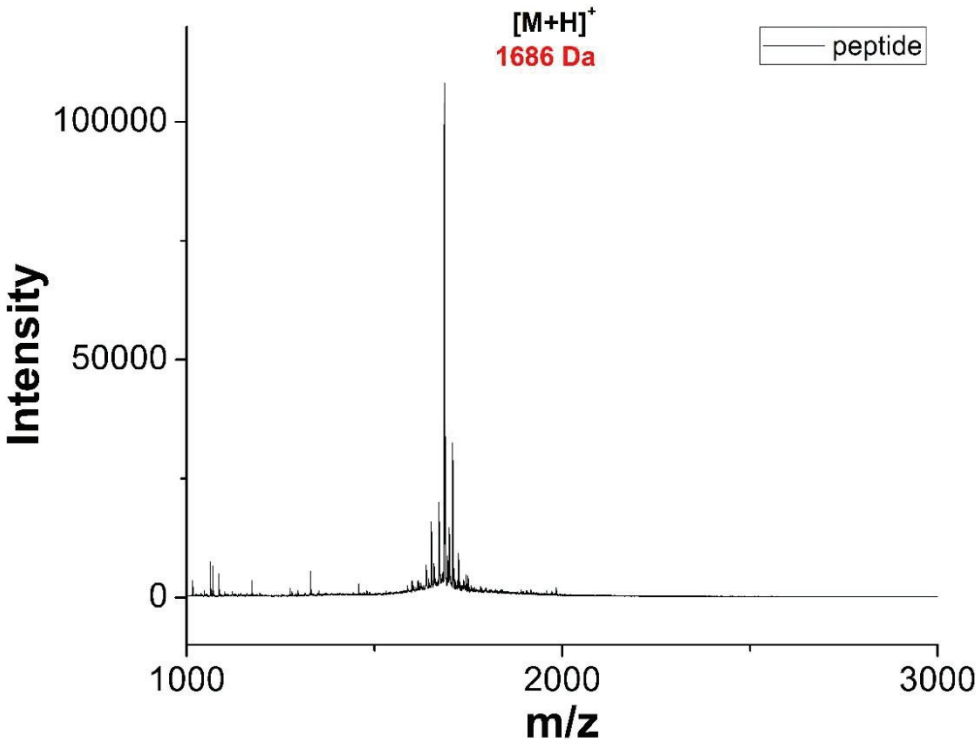

Figure 4.10. MALDI-TOF-MS of the peptide

1664 cm^{-1} and 1666 cm^{-1}, respectively, suggesting that their secondary structure was helical, mainly 3-10 helix (Kong & Yu, 2007)

MALDI-TOF mass spectra of the peptide and the mPEG-peptide are given in Figure 4.10 and Figure 4.11, respectively. In the mass spectrum of the peptide, the peak with the highest intensity, $(M+H)^+$, was observed at 1686 Da, very close to its theoretical molar mass (M = 1682 Da). Along with this peak, a few small peaks related to quite small amount of other peptide impurities were also obtained. 3 Da difference in the experimental and theoretical molar masses of the peptide could be attributed to calibration errors of the instrument. The mPEG-peptide conjugate had broad peaks at ~3500 Da and ~1700 Da corresponding to $(M+H)^+$ and $(M+2H)^{2+}$ species, respectively due to the polydispersity of the mPEG-COOH. Experimental molar mass was very close to the theoretical molar mass of the mPEG-peptide (3582 Da = 1682 Da + 1900 Da) confirming that PEG conjugation was successful.

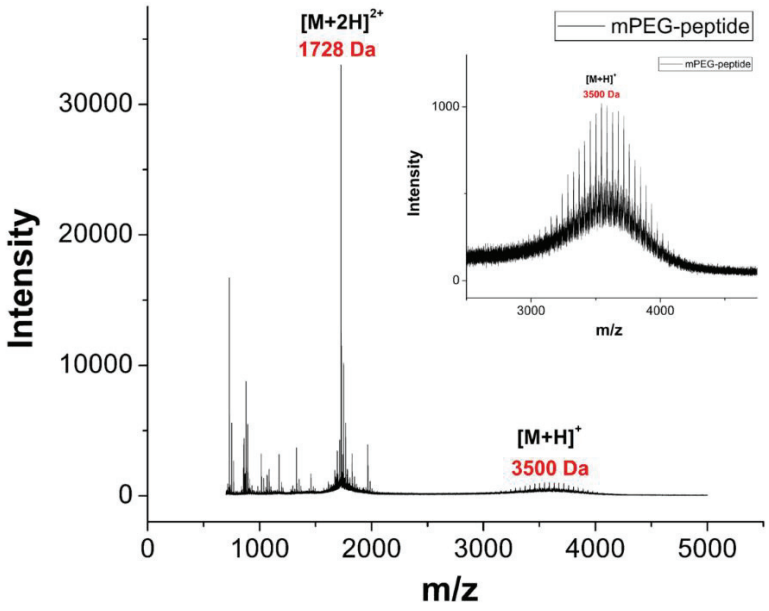

Figure 4.11. MALDI-TOF-MS of the mPEG-peptide

4.3. Characterization of the DOX-Conjugated Drug Delivery Systems

Percent DOX functionalization values of the drug delivery systems were determined by using UV-Vis Spectroscopy. Additionally, drug release profiles, size

distribution and stability of the DOX-conjugated DDSs were determined. These results are given in the following sections.

4.3.1. DOX Content of the DDSs

Percent DOX functionalization values of the mPEG-oxime-DOX were obtained as ~ 48% and ~ 67% according to the respective method 1 and 2 given in Section 3.2.2. For this reason, method 2 was applied to the mPEG-peptide system, and its % DOX functionalization value was obtained as ~77%.

4.3.2. Drug Release

DOX release profiles of the mPEG-oxime-DOX and the mPEG-peptide-oxime-DOX at pH 5.0 and pH 7.4 were investigated for 54 h and are given in Figure 4.12. Maximum % DOX release values of the mPEG-oxime-DOX were obtained as 62.3 ± 0.2 % and 28.7 ± 1.6% for pH 5.0 and pH 7.4, respectively indicating pH programmed release of the drug, attributed to acid cleavable oxime bond. Similar drug release profiles were obtained for mPEG2000-oxime-DOX system developed by Zhang et al., (2016). Lower % release of DOX at pH 5.0 was observed for a mPEG5000-DOX system developed by our group containing another acid cleavable bond, hydrazone bond (Balcı & Top, 2018). The difference may be due to difference in the stability of the bonds and/or in the chain length of the mPEG molecules.

On the other hand, the mPEG-peptide-oxime-DOX exhibited quite low DOX release (~ 15%) independent of pH. Considering acid cleavable property of oxime bond confirmed by the mPEG-oxime-DOX system, it is likely that DOX molecules released could remain attached to the peptide domain via physical interactions such as cation-π interactions and/or H-bonding, which prevented the resultant mPEG-peptide/mPEG-peptide-DOX and released DOX self-assembled system to pass through the dialysis membrane. To confirm this hypothesis, drug release should be monitored by HPLC

system. Indeed, it was recently shown by the docking studies that DOX could interact with an arginine residue of human serum albumin via H-bonding (Shalbafan et al., 2018).

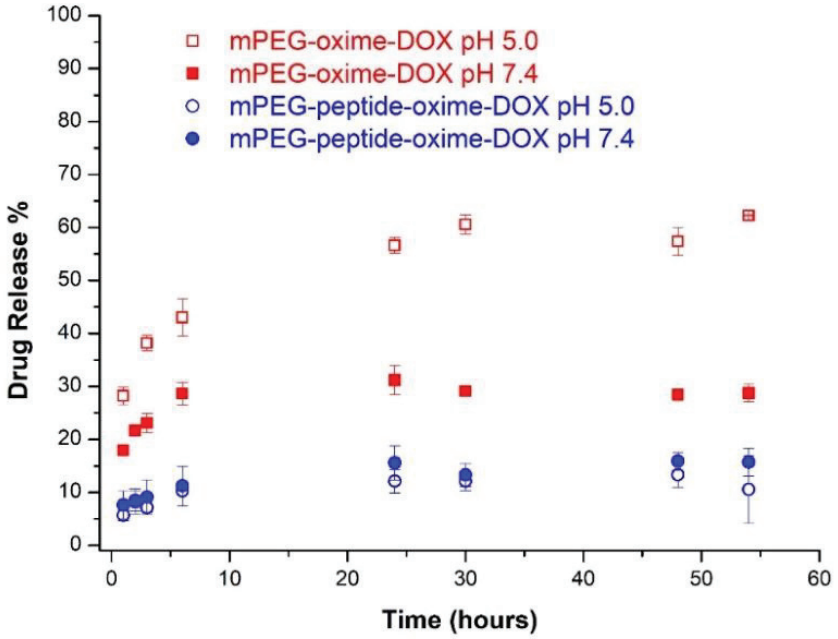

Figure 4.12. DOX release curves the (a) mPEG-oxime-DOX, (b) mPEG-peptide-oxime-DOX obtained at pH 7.4 and pH 5.0.

4.3.3. Size and Stability

Time course size distributions of the mPEG-oxime-DOX and the mPEG-peptide-oxime-DOX at pH 5.0 and 7.4 were determined immediately after dissolution of the DDSs in the buffers and after their incubation at 37°C for 24 h. For the mPEG-oxime-DOX, the results obtained at pH 7.4 and pH 5.0 are given in Figure 4.13 and Figure 4.14, respectively. Corresponding D10, D50 and D90 values are summarized in Table 4.1. Mean size values of mPEG-oxime-DOX at pH 7.4 and 5.0 were obtained as similar, 23 ± 2 nm and 24 ± 4 nm, respectively. Considering the size of mPEG2000 calculated as ~2.6 nm, measured mean size values indicated that DOX attachment triggered the self-assembly of the mPEG-DOX chains. Hydrodynamic diameters of the mPEG5000-hydrazone-DOX and the mPEG5000-amide-DOX systems developed previously in our

group were obtained as 8 ± 1 nm and 17 ± 2 nm, respectively (Balcı & Top, 2018; Şentürk & Top, 2018). Thus, higher mean size values of the mPEG-oxime-DOX can be attributed to its shorter mPEG chain. Size of the mPEG2000-oxime-DOX developed by Zhang et al., (2016), on the other hand, was measured as ~ 160 nm, much higher than that of the mPEG2000-oxime-DOX prepared in this study. The difference can be attributed to differences in sample concentrations and sample preparation methods used in the current thesis and the study of Zhang et al., (2016).

Table 4.1. D10, D50 and D90 values of the mPEG-oxime-DOX

	mPEG-oxime-DOX - pH 5.0		**mPEG-oxime-DOX - pH 7.4**	
	Day 0	**Day 1**	**Day 0**	**Day 1**
D10	17 ± 2	24 ± 1	16 ± 1	38 ± 3
D50	24 ± 4	36 ± 2	23 ± 2	57 ± 4
D90	50 ± 7	71 ± 4	53 ± 4	108 ± 7

After 24 h incubation period, mean size of the sample increased to 36 ± 2 nm at pH 5.0. At pH 7.4, on the other hand, increase in the mean size was higher and reached to 57 ± 4 nm at end of the 24 h. Time-course increasing tendency of hydrodynamic diameter values of the mPEG-oxime-DOX indicated that the self-assembly structures could interact with each other through chain exchange at high temperature (37 ^{o}C) to form larger structures. Initially formed self-assembled structures of the mPEG-hydrazone-DOX and the mPEG-amide-DOX, on the other hand, were found to be stable (Balcı & Top, 2018; Şentürk & Top, 2018). Thus, the higher molecular weight of mPEG chain is necessary to obtain stable structures.

Size distributions of the peptide containing carrier system, mPEG-peptide-oxime-DOX, measured at pH 7.4 and 5.0 are given in Figure 4.15. Estimated D10, D50 and D90 values are given in Table 4.2. Correlation functions are given in Figure A.5 and Figure A.6 in Appendix. Mean sizes of the as prepared samples were obtained as 3 ± 0.4 nm and 6 ± 1 nm at pH 5.0 and pH 7.4, respectively. At pH 5.0, the measured size was very close to the hydrodynamic diameter of mPEG2000 suggesting no self-association

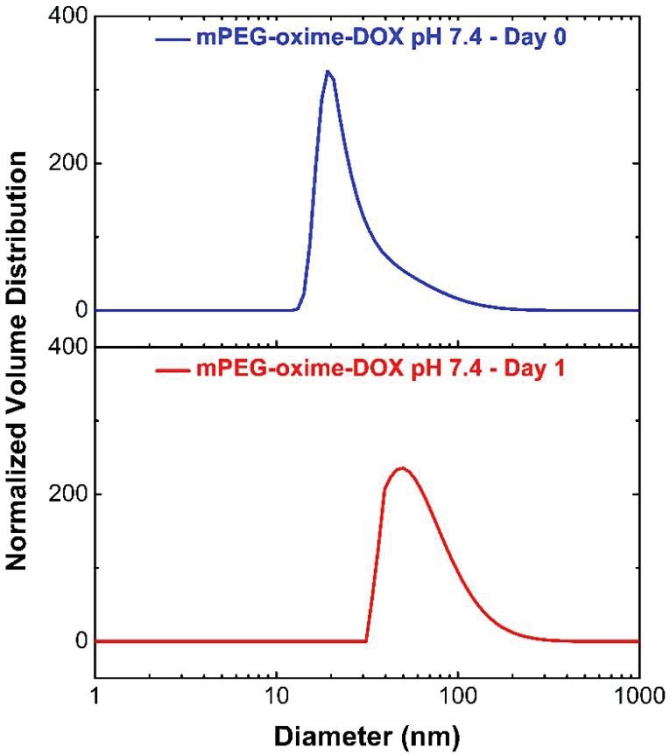

Figure 4.13. Size distributions of the mPEG-oxime-DOX in PBS buffer at pH 7.4 measured immediately and after 1 day

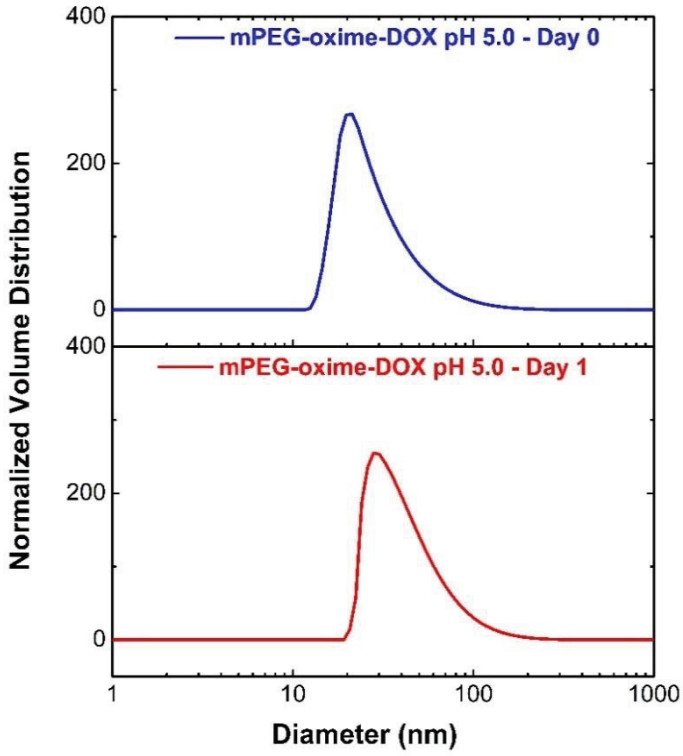

Figure 4.14. Size distributions of the mPEG-oxime-DOX in acetate buffer at pH 5.0 measured immediately and after 1 day

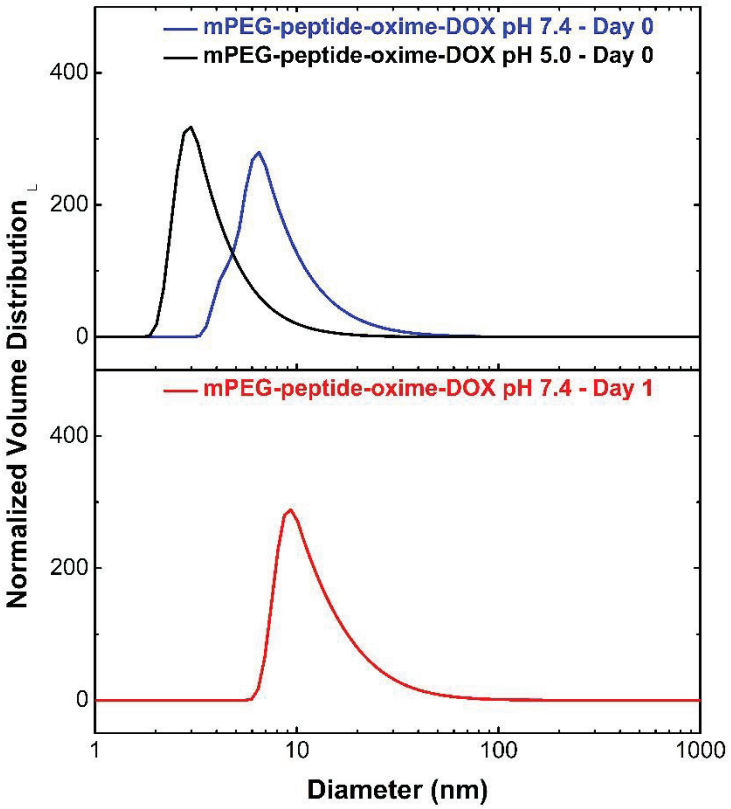

Figure 4.15. Size distribution of the mPEG-peptide-oxime-DOX measured immediately and after 1 day

Table 4.2. D10, D50 and D90 values of the mPEG-peptide-oxime-DOX

	mPEG-peptide-oxime-DOX - pH 5.0		**mPEG-peptide-oxime-DOX - pH 7.4**	
	Day 0	**Day 1**	**Day 0**	**Day 1**
D10	2 ± 0.3	NA	5 ± 0.5	8 ± 0.5
D50	3 ± 0.4	NA	6 ± 1	11 ± 1
D90	6 ± 1	NA	13 ± 1	22 ± 2

between the chains. However, size values doubled at pH 7.4 indicated some degree of aggregation of the mPEG-peptide-DOX at physiological conditions. These size values were quite lower than those measured for the mPEG-oxime-DOX. The difference could be attributed to the repulsions between the positively charged arginines that lowered the self-association between the individual chains. Change in the aggregation state of the

mPEG-peptide-oxime-DOX depending on pH can be explained by the ionization state of DOX. It was reported that DOX had two pKa values at 8.2 and 9.5 (Balcı & Top, 2018). Accordingly, deprotonation of daunosamine group of DOX is higher as pH is increased, resulted in the decrease in the number of positively charged daunosamine groups. Thus, mitigation or elimination of the repulsions between DOX molecules at neutral pH seemed to be the reason for the observed self-association of the mPEG-peptide-DOX at pH 7.4.

CHAPTER 5

CONCLUSIONS AND FUTURE WORK

In this study, mPEG-peptide-oxime-DOX conjugate based drug delivery system was synthesized, characterized, and compared with the control drug delivery system lacking peptide domain. For both configurations, DOX was attached to the carrier molecules via acid cleavable oxime bond. TAT derived cell penetrating peptide was used for the intention of imparting endosome disruption ability to the drug delivery system. In order to conjugate DOX to the carrier molecules, their aldehyde forms were prepared. As the first step, the carrier molecules were oxidized to aldehyde forms using DMSO-acetic anhydride oxidation. FTIR and NMR spectroscopy results of the mPEG-aldehyde synthesized at different conditions indicated that anhydrous conditions were necessary to achieve high level of aldehyde functionalization. mPEG-peptide was synthesized on the resin and its purity was confirmed by HPLC and MALDI-MS. DOX release profiles of the DDSs were obtained at pH 5.0 and pH 7.4. mPEG-oxime-DOX exhibited pH responsiveness by releasing large amount of DOX at acidic pH due to the disruption of the oxime bond. On the other hand, mPEG-peptide-oxime-DOX released very small amount of DOX independent of pH suggesting possible interactions between DOX and peptide domain of the DDS. Size distribution measurements of the mPEG-oxime-DOX indicated self-assembled structures, and the size of the conjugates tended to increase over the time course of measurement. Comparison with the stable self-assembled structures of similar mPEG-DOX conjugates developed in our group indicated that higher molar mass of mPEG is necessary to provide stability to the aggregates of the DDS. Lower mean sizes obtained for the mPEG-peptide-oxime-DOX conjugate in both pH 5.0 and pH 7.4 were attributed to the charge repulsions between arginines in the peptide sequence. Observation of the morphology and evaluation of the cytotoxicity of these DDSs are underway.

APPENDIX A

SUPPLEMENTARY FIGURES

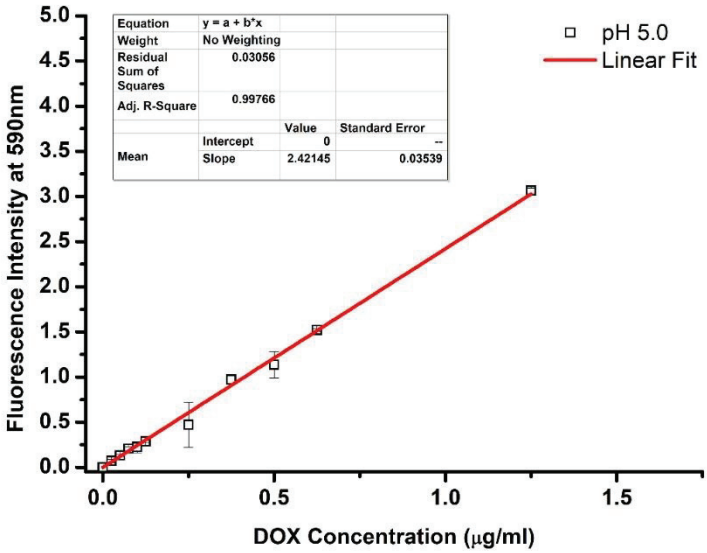

Figure A.1. Calibration curve of free DOX prepared in acetate buffer at pH 5.0

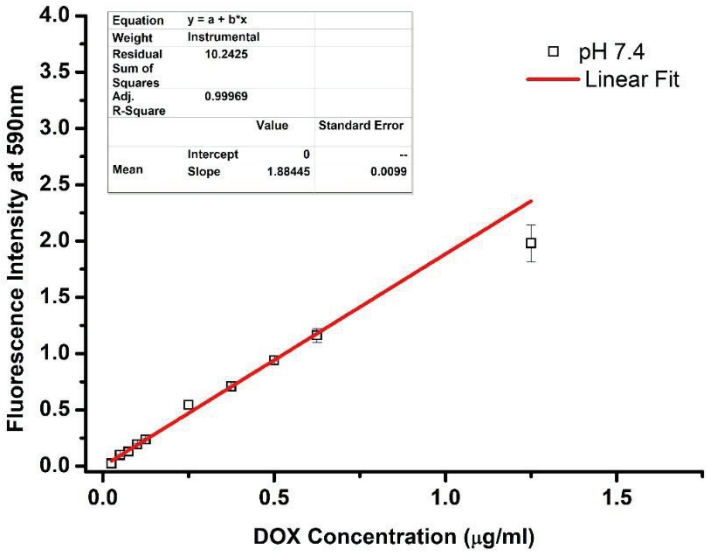

Figure A.2. Calibration curve of free DOX prepared in PBS at pH 7.4

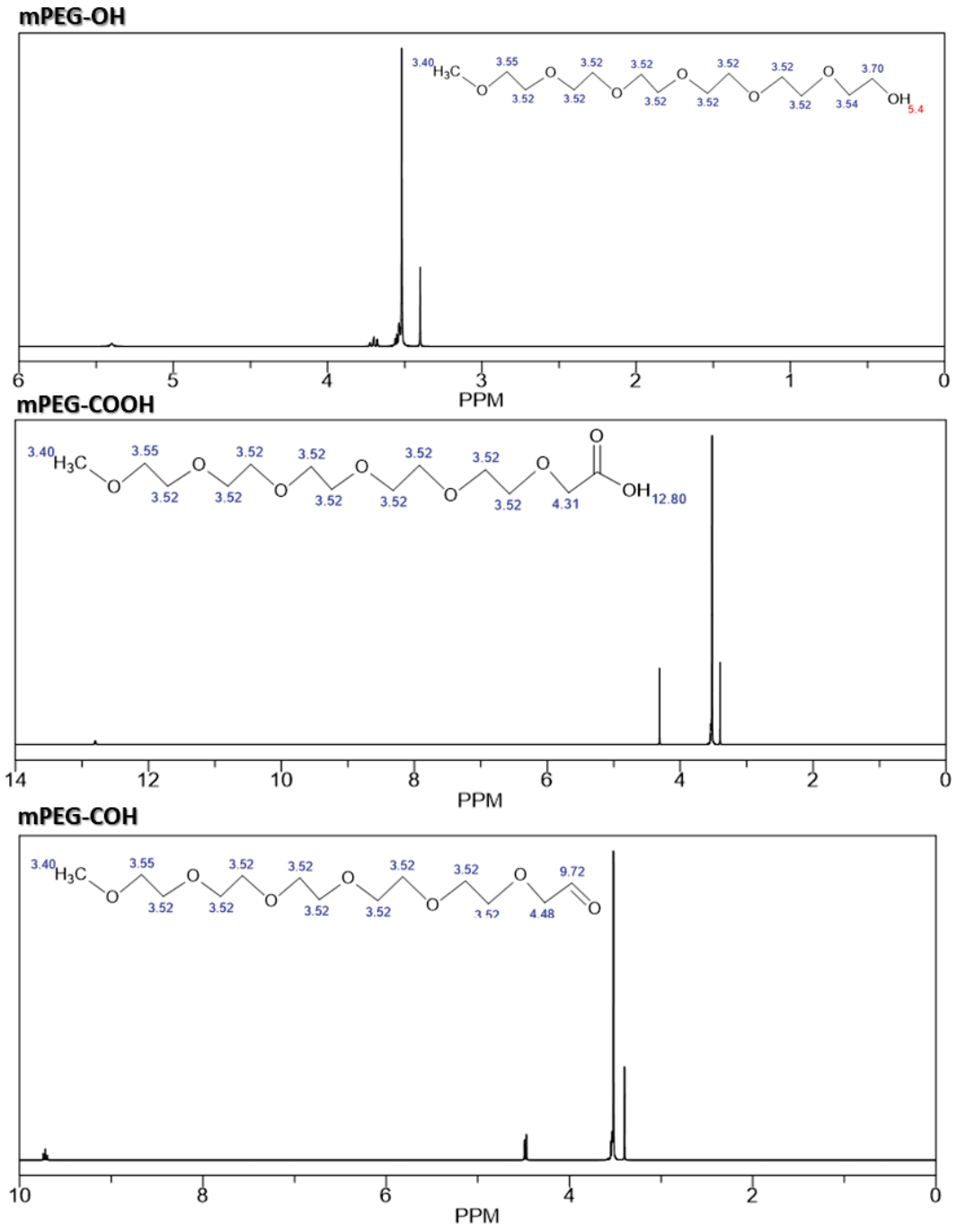

Figure A.3. Theoretical chemical shift values of mPEG-OH, mPEG-COOH, mPEG-COH from H-NMR

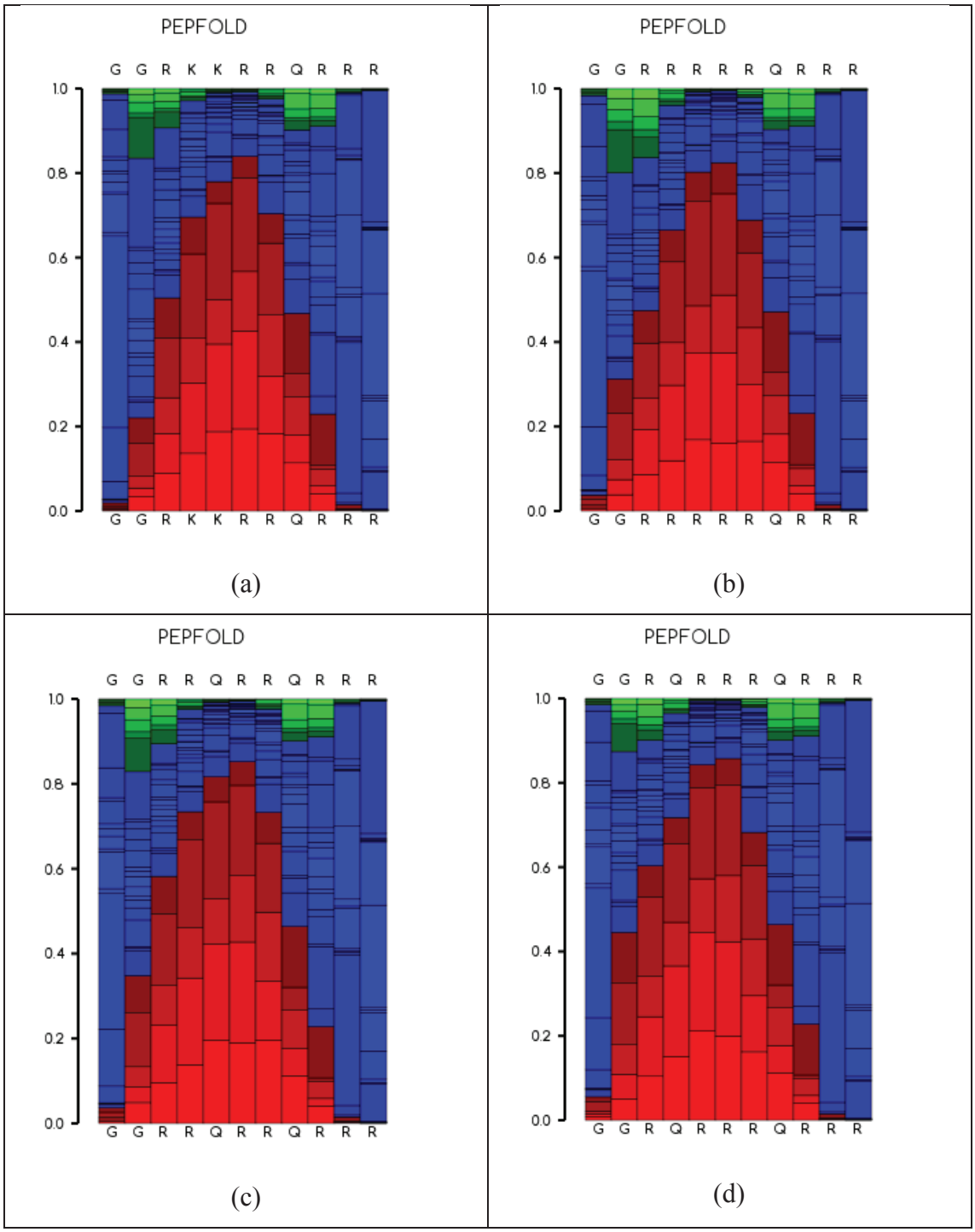

Figure A.4. Secondary structure probability plots of (a) $G_2RKKR_2QR_3G_2S$, (b) $G_2R_5QR_3G_2S$, (c) $G_2R_2QR_2QR_3G_2S$, and (d) $G_2RQR_3QR_3G_2S$ peptides

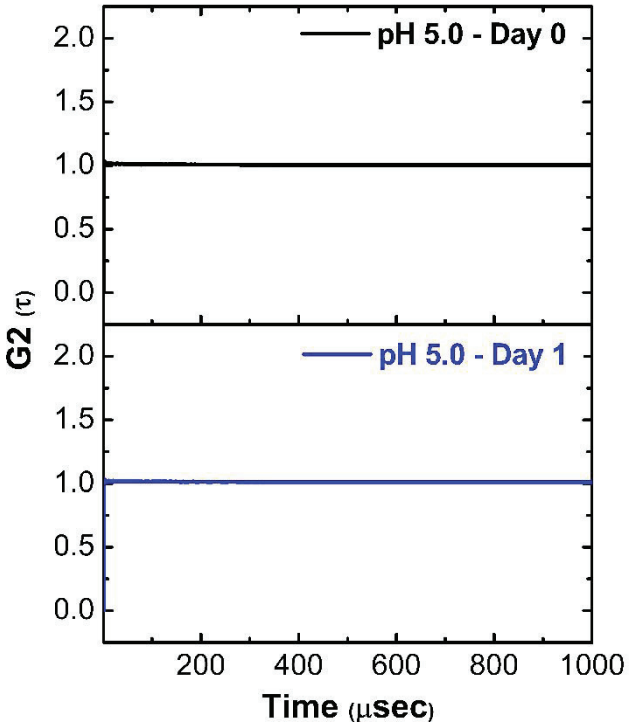

Figure A.5.Correlation functions of the mPEG-peptide-oxime-DOX at pH 5.0

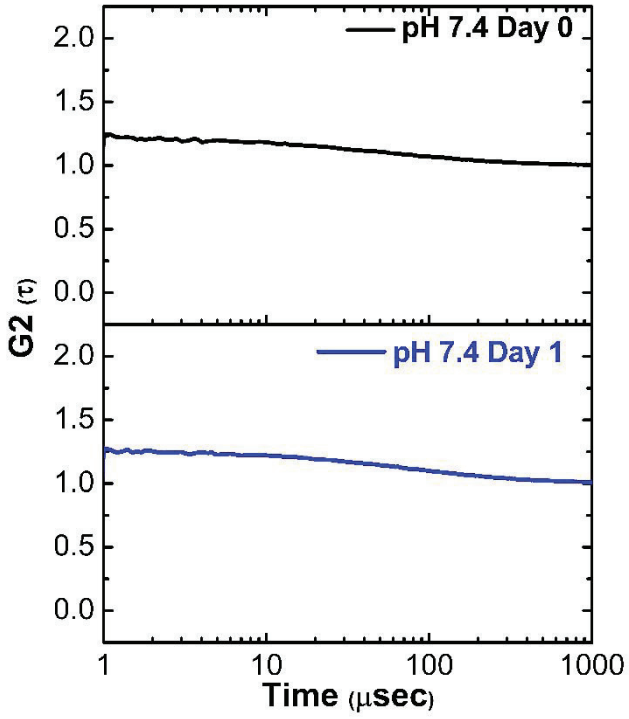

Figure A.6. Correlation functions of mPEG-peptide-oxime-DOX at pH 7.4

APPENDIX B

SAMPLE CALCULATION

% Drug Release Calculation

The sample calculation was performed for the aliquot withdrawn from the release medium at pH 7.4 at the end of 54 h for the mPEG-oxime-DOX carrier system. The data given below were used for calculations.

$C_{conjugate}\left(\frac{mg}{ml}\right)$	1 mg/ml
$V_{conjugate\ in\ membrane}\ (ml)$	0.5 ml
$MW_{DOX}\ \left(\frac{mg}{mmol}\right)$	550 mg/mmol
$MW_{conjugate}\ \left(\frac{mg}{mmol}\right)$	2550 mg/mmol
DOX conjugation %	70%
$V_{dialysis}\ (ml)$	12.5 ml
Dilution factor	4

Fluorescence intensity of the 4 × diluted sample taken at 54 h was measured as 0.851. Slope of the DOX calibration curve at pH 7.4 was determined as 1.884. % DOX release calculation based on these results is as follows:

$$C_t = \frac{0.851}{1.884} \times 12.5\ ml \times 4\ \rightarrow\ C_t = 22.6\ \mu g$$

$$C_i = \frac{1\frac{mg}{ml} \times\ 0.5\ ml \times\ 550\frac{mg}{mmol}}{2450\ \frac{mg}{mmol}} \times 0.70 \times 1000\ \frac{\mu g}{mg}\ \rightarrow C_i = 78.6\ \mu g$$

$$\%\ DOX\ release = \frac{22.60}{78.6} \times 100\ \% = 28.7\ \%$$

REFERENCES

Balcı, Beste and Ayben Top. "Peg and Peg-Peptide Based Doxorubicin Delivery Systems Containing Hydrazone Bond." *Journal of Polymer Research*, vol. 25, 4, 2018.

Bilalis, Panayiotis et al. "Ph-Sensitive Nanogates Based on Poly(L-Histidine) for Controlled Drug Release from Mesoporous Silica Nanoparticles." *Polymer Chemistry*, vol. 7, 7, 2016, pp. 1475-1485.

Böhmova, E. et al. "Cell-Penetrating Peptides: A Useful Tool for the Delivery of Various Cargoes into Cells." *Physiological Research*, 2018, pp. 267-279.

Brigger, Irene et al. "Nanoparticles in Cancer Therapy and Diagnosis." *Advanced Drug Delivery Reviews*, vol. 54, 2002, pp. 631-654.

Brown, J.Martin and Amato J. Glaccia. "The Unique Physiology of Solid Tumors: Opportunities (and Problems) for Cancer Therapy." *Cancer Research*, vol. 58, 1998, pp. 1408-1416.

Carvalho, Cristina et al. "Doxorubicin: The Good, the Bad and the Ugly Effect." *Current Medicinal Chemistry*, vol. 16, 25, 2009, pp. 3267-3285.

Daglioglu, C. "Enhancing Tumor Cell Response to Multidrug Resistance with Ph-Sensitive Quercetin and Doxorubicin Conjugated Multifunctional Nanoparticles." *Colloids Surf B Biointerfaces*, vol. 156, 2017, pp. 175-185.

Drug Delivery Systems. edited by K.K. Jain, Humana Press, 2014.

Feng, Si-Shen and Shu Chien. "Chemotherapeutic Engineering: Application and Further Development of Chemical Engineering Principles for Chemotherapy of Cancer and Other Diseases." *Chemical Engineering Science*, vol. 58, 18, 2003, pp. 4087-4114.

Gong, X. W. et al. "Discarded Free Peg-Based Assay for Obtaining the Modification Extent of Pegylated Proteins." *Talanta*, vol. 71, 1, 2007, pp. 381-384.

Greish, K. "Enhanced Permeability and Retention (Epr) Effect for Anticancer Nanomedicine Drug Targeting." *Methods Mol Biol*, vol. 624, 2010, pp. 25-37.

Guidotti, G. et al. "Cell-Penetrating Peptides: From Basic Research to Clinics." *Trends Pharmacol Sci*, vol. 38, 4, 2017, pp. 406-424.

Harris, J. M. et al. "Synthesis and Characterization of Poly(Ethylene Glycol) Derivatives." *Journal of Polymer Science: Polymer Chemistry Edition*, 1984, pp. 341–352.

Hu, Q. et al. "Enzyme-Responsive Nanomaterials for Controlled Drug Delivery." *Nanoscale*, vol. 6, 21, 2014, pp. 12273-12286.

Hu, X. et al. "Chitosan-Capped Mesoporous Silica Nanoparticles as Ph-Responsive Nanocarriers for Controlled Drug Release." *Chem Asian J*, vol. 9, 1, 2014, pp. 319-327.

Iyer, A. K. et al. "Exploiting the Enhanced Permeability and Retention Effect for Tumor Targeting." *Drug Discov Today*, vol. 11, 17-18, 2006, pp. 812-818.

Kalyane, D. et al. "Employment of Enhanced Permeability and Retention Effect (Epr): Nanoparticle-Based Precision Tools for Targeting of Therapeutic and Diagnostic Agent in Cancer." *Mater Sci Eng C Mater Biol Appl*, vol. 98, 2019, pp. 1252-1276.

Kanamala, M. et al. "Mechanisms and Biomaterials in Ph-Responsive Tumour Targeted Drug Delivery: A Review." *Biomaterials*, vol. 85, 2016, pp. 152-167.

Kaneo, Y. et al. "Preparation and Properties of Acid-Cleavable Poly(Vinyl Alcohol)Cis-Aconityl-Antitumor Anthracycline Conjugates." *Journal of Drug Delivery Science and Technology*, vol. 23, 2, 2013, pp. 143-149.

Kobayashi, H. et al. "Improving Conventional Enhanced Permeability and Retention (Epr) Effects; What Is the Appropriate Target?" *Theranostics*, vol. 4, 1, 2013, pp. 81-89.

Kong, J. and S. Yu. "Fourier Transform Infrared Spectroscopic Analysis of Protein Secondary Structures." *Acta Biochimica et Biophysica Sinica*, vol. 39(8), 2007, pp. 549–559.

Kuang, Tairong et al. "Enzyme-Responsive Nanoparticles for Anticancer Drug Delivery." *Current Nanoscience*, vol. 12, 1, 2015, pp. 38-46.

Lamiable, A. et al. "Pep-Fold3: Faster De Novo Structure Prediction for Linear Peptides in Solution and in Complex." *Nucleic Acids Res*, vol. 44, W1, 2016, pp. W449-454.

Lele, B.S. and M.G. Kulkarni. "Single Step Room Temperature Oxidation of Poly(Ethylene Glycol) to Poly(Oxyethylene)-Dicarboxylic Acid." *Journal of Applied Polymer Science*, vol. 70, 1998, pp. 883-890.

Letchford, K. and H. Burt. "A Review of the Formation and Classification of Amphiphilic Block Copolymer Nanoparticulate Structures: Micelles, Nanospheres, Nanocapsules and Polymersomes." *Eur J Pharm Biopharm*, vol. 65, 3, 2007, pp. 259-269.

Li, Zhen et al. "The Role of Endosome Evasion Bypass in the Reversal of Multidrug Resistance by Lipid/Nanoparticle Assemblies." *Journal of Materials Chemistry B*, vol. 1, 10, 2013,

Lin, J. et al. "Enhanced Antitumor Efficacy and Reduced Systemic Toxicity of Sulfatide-Containing Nanoliposomal Doxorubicin in a Xenograft Model of Colorectal Cancer." *PLoS One*, vol. 7, 11, 2012, p. e49277.

Lin, Y. S. et al. "The Surface Density Gradient of Grafted Poly(Ethylene Glycol): Preparation, Characterization and Protein Adsorption." *Colloids and Surfaces B: Biointerfaces*, vol. 3(1-2), 1994, pp. 49–62.

Liu, J. et al. "Ph-Sensitive Nano-Systems for Drug Delivery in Cancer Therapy." *Biotechnol Adv*, vol. 32, 4, 2014, pp. 693-710.

Liu, Y. et al. "Enzyme Responsive Drug Delivery System Based on Mesoporous Silica Nanoparticles for Tumor Therapy in Vivo." *Nanotechnology*, vol. 26, 14, 2015, p. 145102.

Maeda, H. et al. "A Retrospective 30 Years after Discovery of the Enhanced Permeability and Retention Effect of Solid Tumors: Next-Generation Chemotherapeutics and Photodynamic Therapy--Problems, Solutions, and Prospects." *Microcirculation*, vol. 23, 3, 2016, pp. 173-182.

Mauri, Emanuele et al. "Simple and Efficient Strategy to Synthesize Peg-Aldehyde Derivatives for Hydrazone Orthogonal Chemistry." *Polymers for Advanced Technologies*, vol. 26, 12, 2015, pp. 1456-1460.

Mihanfar, A. et al. "Ovarian Cancer Stem Cell: A Potential Therapeutic Target for Overcoming Multidrug Resistance." *J Cell Physiol*, vol. 234, 4, 2019, pp. 3238-3253.

Mura, S. et al. "Stimuli-Responsive Nanocarriers for Drug Delivery." *Nat Mater*, vol. 12, 11, 2013, pp. 991-1003.

Nakamura, Y. et al. "Nanodrug Delivery: Is the Enhanced Permeability and Retention Effect Sufficient for Curing Cancer?" *Bioconjug Chem*, vol. 27, 10, 2016, pp. 2225-2238.

Naz, Safia et al. "<P>Enzyme-Responsive Mesoporous Silica Nanoparticles for Tumor Cells and Mitochondria Multistage-Targeted Drug Delivery</P>." *International Journal of Nanomedicine*, vol. Volume 14, 2019, pp. 2533-2542.

Pecot, C. V. et al. "Rna Interference in the Clinic: Challenges and Future Directions." *Nat Rev Cancer*, vol. 11, 1, 2011, pp. 59-67.

Prasmickaite, L. et al. "Photochemical Disruption of Endocytic Vesicles before Delivery of Drugs: A New Strategy for Cancer Therapy." *British Journal of Cancer*, vol. 86, 2002, pp. 652-657.

Sang, X. et al. "Preparation and Controlled Drug Release Ability of the Poly[N-Isopropylacryamide-Co-Allyl Poly(Ethylene Glycol)]-B-Poly(Gamma-Benzyl-L-Glutamate) Polymeric Micelles." *Mater Sci Eng C Mater Biol Appl*, vol. 98, 2019, pp. 910-917.

Schmaljohann, D. "Thermo- and Ph-Responsive Polymers in Drug Delivery." *Adv Drug Deliv Rev*, vol. 58, 15, 2006, pp. 1655-1670.

Schmidt, N. et al. "Arginine-Rich Cell-Penetrating Peptides." *FEBS Lett*, vol. 584, 9, 2010, pp. 1806-1813.

Shah, Afzal et al. "Stimuli-Responsive Peptide-Based Biomaterials as Drug Delivery Systems." *Chemical Engineering Journal*, vol. 353, 2018, pp. 559-583.

Shalbafan, M. et al. "Study of Interaction of Human Serum Albumin with Doxorubicin (Anti-Cancer Drug) by Docking Simulation." *Chemical Methodologies*, 2018, pp. 354-359.

Shen, Y. et al. "Improved Pep-Fold Approach for Peptide and Miniprotein Structure Prediction." *J Chem Theory Comput*, vol. 10, 10, 2014, pp. 4745-4758.

Sun, T. et al. "Engineered Nanoparticles for Drug Delivery in Cancer Therapy." *Angew Chem Int Ed Engl*, vol. 53, 46, 2014, pp. 12320-12364.

Şentürk, NesİGÜL and Ayben Top. "Peg-Peptide Conjugate Containing Cathepsin B Degradation Unit as a Doxorubicin Carrier System." *Turkish Journal of Chemistry*, vol. 42, 2, 2018,

Tacar, O. et al. "Doxorubicin: An Update on Anticancer Molecular Action, Toxicity and Novel Drug Delivery Systems." *J Pharm Pharmacol*, vol. 65, 2, 2013, pp. 157-170.

Tai, W. and X. Gao. "Functional Peptides for Sirna Delivery." *Adv Drug Deliv Rev*, vol. 110-111, 2017, pp. 157-168.

Thevenet, P. et al. "Pep-Fold: An Updated De Novo Structure Prediction Server for Both Linear and Disulfide Bonded Cyclic Peptides." *Nucleic Acids Res*, vol. 40, Web Server issue, 2012, pp. W288-293.

Torchilin, V. P. "Micellar Nanocarriers: Pharmaceutical Perspectives." *Pharm Res*, vol. 24, 1, 2007, pp. 1-16.

Treatments & Side Effects. 6th edition edition, CANCER SUPPORT COMMUNITY, 2014.

V. Munsell, Erik et al. "Journey to the Center of the Cell: Current Nanocarrier Design Strategies Targeting Biopharmaceuticals to the Cytoplasm and Nucleus." *Current Pharmaceutical Design*, vol. 22, 9, 2016, pp. 1227-1244.

Varkouhi, A. K. et al. "Endosomal Escape Pathways for Delivery of Biologicals." *J Control Release*, vol. 151, 3, 2011, pp. 220-228.

Wang, H. et al. "Hydrophilic Mesoporous Carbon Nanospheres with High Drug-Loading Efficiency for Doxorubicin Delivery and Cancer Therapy." *Int J Nanomedicine*, vol. 11, 2016, pp. 1793-1806.

Wang, H. et al. "Enhanced Anti-Tumor Efficacy by Co-Delivery of Doxorubicin and Paclitaxel with Amphiphilic Methoxy Peg-Plga Copolymer Nanoparticles." *Biomaterials*, vol. 32, 32, 2011, pp. 8281-8290.

Yin, Q. et al. "Reversal of Multidrug Resistance by Stimuli-Responsive Drug Delivery Systems for Therapy of Tumor." *Adv Drug Deliv Rev*, vol. 65, 13-14, 2013, pp. 1699-1715.

Zhang, Y. et al. "Co-Delivery of Doxorubicin and Curcumin by Ph-Sensitive Prodrug Nanoparticle for Combination Therapy of Cancer." *Sci Rep*, vol. 6, 2016, p. 21225.

Zheng, J. N. et al. "Chitosan-G-Mpeg-Modified Alginate/Chitosan Hydrogel Microcapsules: A Quantitative Study of the Effect of Polymer Architecture on the Resistance to Protein Adsorption." *Langmuir*, vol. 26, 22, 2010, pp. 17156-17164.